Thermal model for analysis of Mars infrared mapping

Hugh H. Kieffer File= /xtex/tes/krc/jpap.tex

July 19, 2010

Contents

July 19, 2010

Liens:

Complete Sections: 4.8, 6
Check Figs 1 and 2
decide on form of IU: $Jm^{-2}s^{-1/2}K^{-1}$or $\mathrm{J\,m^{-2}s^{-1/2}K^{-1}}$

1 Introduction

This paper describes a numerical model used extensively for computing planetary surface temperatures. The KRC numerical model has evolved over a period of four decades and has been used for a variety of planet, satellite and comet problems, but use has concentrated on Mars. The model uses a one-layer atmosphere but does allow condensation and global pressure variation; the model can output surface kinetic and planetary (nadir view from space) bolometric temperatures, along with a variety of parameters related to subsurface-layer and atmosphere temperatures, seasonal polar cap mass, heat-flow and numerical performance parameters.

The program is designed to compute surface and subsurface temperatures for a global set of latitudes at a full set of seasons, with enough depth to capture the annual thermal wave, and to compute seasonal condensation mass. For historic reasons (it originated in the era of kilo-Hz processors) the code has substantial optimization. It allows sloped surfaces and two zones of different sub-surface materials. There are generalities that allow this code set to be used for any ellipsoid with any spin vector, in any orbit (around any star); with or without an atmosphere (including condensation); this is also the source of some of the complexity.

In response to an oft-asked question, the acronym KRC is simply K for conductivity, R for "rho" (ρ) for density, and C for specific heat; the three terms in thermal inertia (TI).

KRC uses explicit forward finite differences and is coded in FORTRAN; model development began 1968, and was used to support the Viking when computing a single case for 19 latitudes at 40 seasons took an hour on a large university main frame computer[1]. For this reason, the code was highly optimized for speed and uses layer thickness increasing exponentially downward and time steps that increase by factors of two deeper into the subsurface where stability criteria are met. The code is modularized based on time scale and function, and there is extensive use of Commons. The version used for Viking was described briefly [appendix] in [34]. The KRC model was used in many analyzes of the Viking IRTM data, derivatives were used to study sublimating comets [65] and ring and satellite eclipses [4, 21]. The code has undergone step-wise revision, a major change being a 2002 replacement of a down-going steady IR flux equivalent to fixed fraction of the noon insolation with the atmosphere described here, in which version it has been the basis for analysis of THEMIS and MER Mini-TES results. The code now allows temperature-dependent thermal conductivity (KofT).

A guide to running KRC is in the file **helplist.txt**; see Supporting material. For THEMIS, a "one-point" capability was included that allows input of a set of points defined by season, latitude, hour and a few major physical parameters; KRC will produce the surface kinetic temperature and planetary brightness temperature for these points; see Section 4.10.

1.0.1 Use for recent missions

Although the thermal models for the MGS Thermal Emission Spectrometer (TES) data production were based on the Mellon-Jakosky-Haberle model, which has some heredity from KRC [39, 51], KRC has been used in the analysis of TES data [40, 41]. Extensive comparison of the Mellon model and KRC was done in development of the MGS TES production code.

Determination of thermal inertia using the KRC model has been used in selecting all landing sites on Mars; Pathfinder: [25], MER: [14, 27], Phoenix: [1], MSL: (M. Golombek, personal communication). Post-landing assessment has shown the forecasts of rock abundance to be close [24, 23].

Standard data reduction of the Odyssey Thermal Emission Imaging System (THEMIS) uses the KRC model,[12, 13, 53, 61]. KRC was used in analysis and surface thermal observations by Mini-TES, [26, 19].

KRC thermal modeling has been used for study of general nature of the Martian surface [5, 6, 7, 17, 3], Chapter 9 in [10]; and detailed sites: [2, 15, 18, 19, 20, 22, 28, 54].

[1] An IBM 360-91, at that time the largest (4 Mbyte memory) and fastest (16 * 1 MIPS) un-classified computer

KRC models are the basis for the surface temperature estimate to be used for the black-body emission correction to Mars Reconnaissance Orbiter (MRO) Compact Reconnaissance Imaging Spectrometer for Mars(CRISM) reflection spectra, [38].

KRC [32] and derivatives [47, 48] have been used in study of seasonal slab ice. The capability to model temperatures at the bottom of conical pits was added to study the potential volatile sublimation in freshly exposed trenches to be dug by the Phoenix mission.

1.0.2 Some other thermal models used for Mars

A finite-difference thermal model used for estimating depth to liquid water stability [16] was made publicly available. A derivative of this model and KRC was used to study ground ice stability [43].

The martian atmosphere has a significant effect on surface temperature, both in the physical temperature of the surface being influenced by the dusty atmosphere's modification of the insolation that reaches the surface, and on the apparent temperature measured remotely by infrared radiometry [29]. Thermal models which treat the atmosphere in detail, such as a dusty radiative/convective column [29] or that include lateral heat transport such in a General Circulation Model (GCM) [30, 8], generally take two to several orders of magnitude longer to compute.

The model used by the U. Colorado group [39] has indirect heritage from KRC and uses a similar subsurface, but has a multi-layer radiative/convective atmosphere; this model was used for TES standard data production.

The goal of the KRC model has been to account for the first-order effects of the atmosphere, while preserving the speed and flexibility to deal with surface effects such as layered materials and sloping surfaces. A complicating factor in treating the atmosphere more fully is that the opacity of Mars's atmosphere can vary considerably in space and time [59], only GCM's with surface dust interaction model this.

A model similar to KRC was used largely for Mars' polar studies [46, 44, 45].

1.0.3 Notation here

Program and routine names are shown as **PROGRM [,N]** , where **N** indicates a major control index. Code variable names are shown `VARIAB`. Input parameters are shown as INPUT. File names are shown as *file*.

For convenience, some physical parameter default values are shown within square brackets at their point of mention and some are listed in Table 1. All units are SI, except the use of days for orbital motion. The sample input file (Appendix A), includes all input parameters.

2 Physical representation

2.1 Planetary Orientation and Orbit

KRC can accept either fixed heliocentric range and sub-solar latitude, or Keplerian orbital elements and a fixed planet orientation (direction of the spin axis); in both cases, "seasons" are at uniform increments of time. An associated Planetary ORBit program set, **PORB**, main program **porbmn**, accesses files containing the elements for all the planets [57] and a few comets and minor planets ; this program set pre-calculates the orbital elements for any epoch, converts them into rotation matrices for the chosen epoch and creates an ASCII parameter set that is then incorporated into the input file for KRC. For TES and the initial THEMIS modeling, the martian elements were evaluated for epoch 1999; Mars' spin-axis orientation was based on pre-Viking data, and differs from the current best estimates [56] by about 0.3°. Within KRC, the orbital position of Mars is computed for each "season", yielding the heliocentric range, the sub-Solar latitude, and the seasonal indicator L_s.

Planetary orientations have been updated to [56] and mean elements have been updated to [55].

For Mars, the maximum error in ecliptic longitude is under 30 arc-sec, corresponding to about 1/60 of a sols' motion, which is negligible compared to the assumption of ignoring Martian longitude.

2.2 Atmosphere

KRC uses a one-layer atmosphere that is gray in the solar and thermal wavelength ranges. Radiative exchange with the Sun, space and the surface determines the atmosphere energy balance and its temperature variation. The columnar mass (and the surface pressure) can vary with season and surface elevation. A uniformly-mixed dust loading is allowed to modify the visual and thermal opacity. Direct and diffuse illumination are computed using a double-precision 2-stream Delta-Eddington model, with single scattering albedo ϖ and Henyey-Greenstein asymmetry parameter G_H. The thermal opacity is a constant factor C_2 times the visual opacity. An option allows an extension of twilight past the geometric terminator.

The current local solar-wavelength atmospheric opacity of dust, τ, can vary with atmospheric pressure: $\tau = \tau_0 \cdot P/P_0$

2.2.1 Delta Eddington 2-stream

A Delta-Eddington model is used for atmosphere scattering and fluxes (**deding2.f**); output parameters are normalized to unit solar irradiance along the incident direction at the top of atmosphere; so they must be multiplied by S_M to get flux.

Scattering parameters used are the aerosol single scattering albedo ϖ and the scattering asymmetry parameter [31]; both are input constants. The computed values include:

Planetary (atm plus surface system) albedo: `BOND`
Direct beam at the bottom, includes both collimated and aureole: $F_\parallel$ = `COLL`
Diffuse irradiances: $I_{i,j}$ =
i: [1, = isotropic [2, = asymmetric
j: ,1]= at top of atmosphere ,2] = at bottom of atm

The net diffuse flux is $F_\ominus = \pi[I_{1j} \pm \frac{2}{3} I_{2j}]$ where + is down, $F_\ominus^\downarrow$; - is up, $F_\ominus^\uparrow$. [58, eq. 8]

The total down-going solar flux through the day at the bottom of the atmosphere is

$$S_t' = S_M \left(\cos i_0 \; F_\parallel + F_\ominus^\downarrow \right) \qquad \text{eq : st} \tag{1}$$

where the diffuse component is $F_\ominus^\downarrow = \pi \left(I_{1,2} + \frac{2}{3} I_{2,2} \right)$

Solar heating of the atmosphere, by conservation of energy, is

$$H_V = S_M \left(\mu_0 - F_\ominus^\uparrow(0) - (1 - A_s) \left[\mu_0 \; F_\parallel + F_\ominus^\downarrow(\tau) \right] \right) \qquad \text{eq : aheat} \tag{2}$$

where $\mu_0 \equiv \cos i_0$.

2.2.2 Twilight

Twilight is allowed to account for having a turbid atmosphere. It is implemented as having the diffuse downward illumination depend upon an incidence angle scaled to go to 90° when the Sun is `TWILI` below the geometric horizon.

Because of the twilight extension, there can be a small negative energy balance near twilight. Physically, this is lateral scattering and does not strictly fit a one-layer model. There is no solar heating of the atmosphere during twilight.

2.2.3 Atmospheric IR radiation

The IR opacity is approximated as $\tau_R = P/P_0 \cdot (C_1 + C_2 \tau)$ where C_1 represents the opacity of the "clear" atmosphere, primarily due to the 15μm band, and C_2 is the IR/visual opacity ratio for dust.

The fractional thermal transmission of the atmosphere at zenith is roughly $e^{-\tau_R}$. The fractional absorption is $\beta \equiv 1. - e^{-\tau_R}$.

The fractional transmission of planetary (thermal) radiation in a hemisphere is:

$$e^{-\tau_e} \equiv \int_0^{90} e^{-\tau / \cos\theta} \cos\theta \sin\theta \; d\theta \tag{3}$$

Numerical integration shows that the effective hemispheric opacity is, within about 0.05 in the factor,

$$\tau_e \sim [1.0 < (1.50307 - 0.121687 * \ln \tau_R) < 2.0]\, \tau_R; \tag{4}$$

this is used in the effective absorption $\beta_e \equiv 1. - e^{-\tau_e}$.

The hemispheric downward (and upward) emission from a gray slab atmosphere is: $R_\Downarrow = \sigma T_a^4 \beta_e$. The IR heating of the atmosphere is:

$$H_R = \epsilon\sigma T_s^4(1. - e^{-\tau_e}) - 2R_\Downarrow \quad = \quad \sigma\beta_e(\epsilon T_s^4 - 2T_a^4) \qquad \text{eq : rheat} \tag{5}$$

To estimate the back-radiation from a clear atmosphere, a synthetic transmission spectrum of the Mars atmosphere with a nominal amount of water vapor (provided by David Crisp) was multiplied by blackbody spectra for a range of temperatures to determine the fraction of radiation blocked, see Figure 3. A coefficent of $C_1 = 0.11 \pm 0.004$ covers the range 187K to 293K.

2.2.4 Atmospheric temperature

The atmospheric temperature is assumed to follow radiative energy conservation:

$$\frac{\partial T_a}{\partial t} = \frac{H_R + H_V}{c_p M_a} \qquad \text{eq : dTa} \tag{6}$$

where $M_a = P/G$ is the mass of the atmosphere and c_p is its specific heat at constant pressure.

Because the atmospheric temperature variation has significant time lag relative to the surface, one can use the surface temperature from the prior time step (typically 1/384 of a sol) with little error.

If the computed atmospheric temperature at midnight drops below the CO_2 saturation temperature for one scale height above the local surface, it is bounded at this value and the excess energy loss is converted to snow. If there is frost on the ground, this snow mass is added to the frost; otherwise it is ignored in the heat budget, which strictly does not conserve energy.

$$\Delta M = \Delta T c_p M_a / L \qquad \text{eq : dMa} \tag{7}$$

The nadir planetary temperature is given by

$$\sigma T_P^4 = \epsilon\sigma T_S^4(e^{-\tau_R}) + \sigma T_a^4(1 - e^{-\tau_R}) \implies T_P = \left[\epsilon(1. - \beta)T_S^4 + \beta T_a^4\right]^{1/4} \qquad \text{eq : Tp} \tag{8}$$

2.3 Geometry and Starting Conditions

2.3.1 Geometry

The diurnal variation of insolation onto the surface at the bottom of the atmosphere is computed for the current season and latitude. The incidence angle from zenith onto the horizontal plane (i_0) or sloped surface is computed by:

$$\cos i = \sin\delta \sin(\theta + s_N) - \cos\delta \cos(\theta + s_N) \cos(\phi + s_E) \tag{9}$$

where

δ = the solar declination,
θ = latitude,
ϕ = hour angle from midnight,
s_N = north component of surface slope,
s_E = east component of surface slope,

Direct (collimated) insolation is computed for the local surface, which may be sloped in any direction and has incidence angle i_2;

Direct insolation is zero when either i_0 or i_2 is $> 90°$. Diffuse illumination is based on i_0, with the optional extension into twilight (see Section 2.2.2). For a sloped surface, the solid angle of skylight is reduced and light reflected off

the regional surface (presumed Lambert and of the same albedo) is added; the Delta-Eddington downward diffuse radiance is multiplied by `DIFAC` $= 1 - \alpha + \alpha A$, where $\alpha = (1 - \cos i_2)/2$ is the fraction of the upper hemisphere obscured by ground. For the small flat bottom of conical pits, $\alpha = \sin^2\left(\frac{\pi}{2} - s\right)$ where s is the slope of the pit wall from horizontal.

If a sloping surface (or pit) is used, the regional horizontal surface (or pit wall) is assumed to be at the same temperature, which becomes a poor approximation for steep slopes.

The incident flux at the top of atmosphere is: $I = S_M \cos i_0$, where $S_M \equiv \frac{S_o}{U^2}$, S_o is the solar constant and U is heliocentric range of Mars in Astronomical Units..

2.3.2 Starting conditions: Diurnal-average equilibrium

For the first season, the atmosphere temperature is set based on the equilibrium for no net heating of the atmosphere or surface, using the diurnal average of insolation (see Eq. 2 and Eq. 5):

$$\langle H_V \rangle + \langle H_R \rangle = 0 \qquad \text{eq : VR} \tag{10}$$

Surface radiation balance, from Eq. 13 for a flat surface with no net sub-surface heat flow:

$$\epsilon\sigma\langle T_s^4 \rangle = (1. - A)\langle S'_{(t)} \rangle + \epsilon\sigma\beta_e\langle T_a^4 \rangle \qquad \text{eq : sbal} \tag{11}$$

Expansion of $\langle H_R \rangle$ using Eq. 5 and substitution into Eq. 11, yields ;

$$\langle T_a^4 \rangle = \frac{\langle H_V \rangle/\beta_e + (1 - A)\langle S'_{(t)} \rangle}{\sigma(2 - \epsilon\beta_e)} \qquad \text{eq : Ta4} \tag{12}$$

Substitute into Eq. 11 to get $\langle T_s \rangle$. For computational simplicity, the average top-of-atmosphere insolation is used as an approximation for $\langle S'_{(t)} \rangle$; this slightly over-estimates the temperature of the atmosphere at the start of the first season.

The planetary heating values are based on the average surface temperatures from the prior season; this is similar to allowing some long-term lag in total atmospheric temperature response.

2.4 CO_2 Frost condensation and Sublimation

The local frost condensation temperature `TFNOW` may be either fixed at an input value `TFROST`, or derived from the local surface partial pressure at the current season.

The relation between condensation/sublimation temperature and partial pressure is taken to be the Clausius-Clapeyron relation: $\ln P_c = a - b/T$, in **CO2PT** with a=27.9546 [Pascal] and b=3182.48 [1/Kelvin], derived from [33] page 959.

If frost is present, $E = W \cdot \Delta t$ energy is used to modify the amount of frost; $\Delta M = -E/L$, where L is the latent heat of sublimation. The frost albedo may depend upon insolation, and there may be an exponential attenuation of the underlying ground albedo; see §2.4.1. The amount of frost at each latitude is carried (asymptotic prediction) to the next season.

2.4.1 Effective Albedo

A thick frost deposit can have a constant albedo, or be linearly dependent upon the insolation as described by [42, 35]. It should be noted that it is now known that regions of the seasonal caps can have virtually constant low albedo, [35, 62].

As the seasonal frost thins, the effective albedo of the surface continuously approaches that of underlying soil. $A = A_f + (A_s - A_f)e^{-M/M_e}$ where M_e is the frost required, kg m^{-2}, for unity scattering attenuation..

2.4.2 Global and local pressure

The total amount of atmosphere is set by the annual mean surface pressure at the reference elevation, P_0, input as PTOTAL.
The current global pressure P_g =PZREF, can be any of the following:
1) constant at P_0
2) P_0 times the normalized Viking Lander pressure curve VLPRES [60]
3) Based on depletion of atmospheric CO_2 by growth of frost caps; P_0 minus the total frost mass at the end of the prior season. Requires that the number of latitudes NLAT> 8.

The initial partial pressure of CO_2 at zero elevation is $P_{c0} = P_0 \cdot (1.-$non-condensing fraction) =PCO2M. The current CO_2 partial pressure at zero elevation is $P_{cg} = P_{c0} + (P_g - P_0)$ =PCO2G.

Both the current local total pressure and CO_2 partial pressure scale with surface elevation and scale height: $P \propto e^{-z/\mathcal{H}}$. The scale height is: $\mathcal{H} = T_a\mathcal{R}/\mathcal{M}G$; where T_a is the mean atmospheric temperature over the prior day (or season), $\mathcal{R}$ is the universal gas constant, $\mathcal{M}$ is the mean molecular weight of the atmosphere (43.5), and G is the martian gravity.

Local current dust opacity scales with local total pressure: $\tau = \tau_0 \cdot P/P_0$. The atmospheric saturation temperature is evaluated at one scale height above the local surface.

2.5 Boundary conditions

2.5.1 Level Surface

The surface condition for a frost-free level surface is :

$$W = (1. - A)S'_{(t)} + \Omega\epsilon R_{\Downarrow} + \frac{k}{X_2}(T_2 - T) - \Omega\epsilon\sigma T^4 \qquad \text{eq : w} \tag{13}$$

where W is the heat flow into the surface, A is the current surface albedo, $S'_{(t)}$ is the total solar radiation onto the surface as in Eq. 1, $R_{\Downarrow}$ is the down-welling thermal radiation (assumed isotropic), k is the thermal conductivity of the top layer, X_2 is the depth to the center of the first soil layer, and T is the kinetic temperature of the surface. Most constant terms are pre-computed, see Table 1. Ω is the visible fraction of the sky; for level surfaces, $\Omega = 1$. In the absence of frost, the boundary condition is satisfied when W=0.

When frost is present, the values in Eq. 13 are replaced with ϵ_F, A_F, and T_F, where subscript F indicates the frost values, and no iteration is done; leaving W as a non-zero quantity to change the frost amount. See Section 2.4.

2.5.2 Slopes and Conical Holes

The surface condition for a planar sloped surface or a conical pit with a small flat bottom modifies the interaction with the radiation field. This is simplified by using the crude approximation that the surfaces visible to the point of computation are at the same temperature and have the same brightness where illuminated. Then

$$S'_t = S_M \left[F_{\parallel}\cos i_2 + \Omega F^{\downarrow}_{\ominus} + \alpha A(G_1 F_{\parallel} + \Omega F^{\downarrow}_{\ominus})\right] \qquad \text{eq : pit} \tag{14}$$

$F_{\parallel}$ is the collimated beam in the Delta-Eddington model and $F^{\downarrow}_{\ominus}$ is the down-going diffuse beam. G_1 is the fraction of the visible surrounding surface which is illuminated. Within the brackets in Eq. 14,
the first term is the direct collimated beam, DIRECT
the second is the diffuse skylight directly onto the target surface, DIFFUSE
the third term is light that has scattered once off the surrounding surface, BOUNCE

For a sloped surface, G_1 is taken as unity. As a first approximation, for pits $G_1 = (90 - i)/s \ < 1)$ where s is the slope of the pit walls. For a flat-bottomed pit, $i_2 = i$ when the sun is above the pit slope, and $\cos i_2 = 0$ when below.

2.5.3 Physical properties, Layering of materials and sub-surface scaling

All physical properties are specified by parameters in the input file. Nominal planetary parameters for Mars are the mean solar day, 1.0275 days, and the surface gravity, 3.727 m s^{-2}. Properties of the upper-layer material are specified by the specific heat C_p [J/(kg K)], density ρ [kg/m^3] and thermal inertia I [J m^{-2} $s^{-frac12}$ K^{-1}], which in turn sets the conductivity k [W/(K m)]

Beginning with layer IC, all lower layers can have their conductivity, density and volume specific heat reset to COND2, DENS2, and SPHT2 respectively. If LOCAL is set true, then the physical thickness of these layers scales with the local thermal diffusivity; otherwise, the geometric increase of physical layer thickness continues downward unaltered.

2.5.4 Base of model

Normally, the base of the model is treated as insulating. However, there are also options for it to be held at a fixed temperature, which is useful to model subsurface H_2O ice.

2.6 Relation of thermal inertia to particle size

The relation of TI to particle diameter is based on laboratory measurements,[49]; the specific relation shown in Figure 8 is for P=600 Pascal, density=1600 kg/m^3 and specific heat=625.

A histogram was made of the Thermal inertia determined from TES global map data, [50], although this used a different thermal model. The TI source data are available at http://lasp.colorado.edu/inertia/2007/ ; these data were weighted by area. Most areas are in TI range of 100:500; values above about 200 are increasingly affected by a rock population or real bedrock.

3 Numerical Methods

The addition of temperature-dependent conductivity is treated as a variation to the constant-conductivity version.

3.1 Basic Method

The user inputs the thermal inertia I, the bulk density ρ, and the specific heat of the material C_p. Thermal conductivity k is computed from $I^2/(\rho C_p)$. The thermal diffusivity is $\kappa = \frac{k}{\rho C_p}$. While k, ρ, and C_p do not independently influence the surface temperature for a homogeneous material, they set the spatial scale of the subsurface results; $\texttt{SCALE} = \sqrt{kP/\pi\rho C_p}$.

KRC uses layers that increase geometrically in thickness by a factor RLAY. In order to simplify the innermost code loops, KRC places the radiating surface between the first and second model layers.

Symbols used:

B_i = thickness of layer i [m]. Top (virtual) layer = FLAY * SCALE.
C_p specific heat of the material
H = heat flow=$-k\frac{dT}{dz}$
i = layer index, layer 1 is above the physical surface
subscript +(-) is shorthand for $i+(-)1$; i+.5 is the lower boundary of the layer
I = thermal inertia $\equiv \sqrt{k\rho C_p}$
k = thermal conductivity
P = PERSEC = diurnal period in seconds
R = RLAY = ratio of thickness of succeeding layers
t = time
T = temperature
X = X = depth to middle of each layer [m]
ρ = bulk density
κ = Thermal diffusivity $\equiv \frac{k}{\rho C_p}$

Basic differential equation of heat flow is :

$$\frac{\partial T}{\partial t} = \frac{-1}{\rho C_p}\frac{\partial}{\partial z}\left(-k\frac{\partial T}{\partial z}\right) \quad = \quad \frac{k}{\rho C_p}\frac{\partial^2 T}{\partial z^2} \tag{15}$$

Expressed for numerical calculations:

$$\frac{\Delta T_i}{\Delta t} = -\frac{H_{i+1/2} - H_{i-1/2}}{B_i \rho_i C_{p_i}} \tag{16}$$

Use steady-state relations to find heat flow at interface between two layers: $H = -k\nabla T$

$$H_{i+.5} = -\frac{T' - T_i}{B_i/2}k_i \quad \text{or} \quad T' - T_i = -\frac{H_{i+.5}B_i}{2k_i} \tag{17}$$

where T' is the temperature at the interface.

$$\text{similarly} \quad T_{i+1} - T' = -\frac{H_{i+.5}B_{i+1}}{2k_{i+1}}$$

$$\text{Thus} \quad T_{i+1} - T_i = -\frac{H_{i+.5}}{2}\left(\frac{B_i}{k_i} + \frac{B_{i+1}}{k_{i+1}}\right)$$

$$\text{or} \quad H_{i+.5} = -\frac{2(T_{i+1} - T_i)}{\frac{B_i}{k_i} + \frac{B_{i+1}}{k_{i+1}}} \qquad \text{Similarly} \qquad H_{-.5} = -2\frac{T - T_-}{\frac{B}{k} + \frac{B_-}{k_-}}$$

For uniform layer thickness in uniform material, the standard form of explicit forward difference is

$$\frac{\Delta T_i}{\Delta t} = \frac{\kappa}{B^2}\left[T_+ - 2T_i + T_-\right]$$

3.2 Finite difference scheme for Exponential layer thickness

The depth parameter is scaled to the diurnal thermal skin depth. For variable layer thickness:

$$\frac{\Delta T_i}{\Delta t_i} = \frac{2}{B_i \rho_i C_{p_i}} \left[\frac{T_+ - T_i}{\frac{B_i}{k_i} + \frac{B_+}{k_+}} - \frac{T_i - T_-}{\frac{B_i}{k_i} + \frac{B_-}{k_-}} \right] \tag{18}$$

Formulate as

$$\Delta T_i = F_{1_i} \left[T_+ + F_{2_i} T_i + F_{3_i} T_- \right] \qquad \text{eq : deltaT} \tag{19}$$

Define intermediate constants for each layer:

$$F_{1_i} = \frac{2\Delta t_i}{B_i \rho_i C_{p_i}} \cdot \frac{1}{\frac{B_i}{k_i} + \frac{B_+}{k_+}} \equiv \frac{2\Delta t_i}{\rho_i C_{p_i} B_i^2} \cdot \frac{k_i}{1 + \frac{B_+}{B_i}\frac{k_i}{k_+}} \qquad \text{eq : F1} \tag{20}$$

and

$$F_{3_i} = \left(\frac{B_i}{k_i} + \frac{B_+}{k_+} \right) \cdot \frac{1}{\frac{B_i}{k_i} + \frac{B_-}{k_-}} \equiv \frac{1 + \frac{B_+}{B_i}\frac{k_i}{k_+}}{1 + \frac{B_-}{B_i}\frac{k_i}{k_-}} \qquad \text{eq : F3} \tag{21}$$

and

$$F_{2_i} = -(1 + F_{3_i}) \qquad \text{eq : F2} \tag{22}$$

Then the inner-most loop is Eq. 19 followed by

$$T_i = T_i + \Delta T_i \tag{23}$$

The input parameter FLAY specifies the thickness of the top "virtual" layer is dimensionless units (in which the diurnal skin depth is 1.0), so that the scaled thickness of the uppermost layer in the soil is FLAY*RLAY, and the physical depth of its center in meters is 0.5*FLAY*RLAY*SCALE. Normally (LP2 set true) a table of layer thickness, depth, (both scaled and in meters), overlying mass, and numerical convergence factor is printed out at the start of a run.

3.2.1 Extension to temperature-dependent properties

Temperature-dependent properties must be evaluated at each layer and time-step.

Because conductivities and layer thicknesses appear largely as ratios, KRC calculates these as infrequently as possible. $k_{(T)}$ is implimented as a third-degree polynomial; expecting that the linear and quadratic term will cover the variation in gas conductivity and the cubic term the radiation effect. To minimize roundoff problems, the polynomial uses a scaled independant variable $T' = (T - T_{off}) * T_{mul} = (T - 220.) * 0.01$. Because KRC allows two materials, this requires 8 coefficients.[Implemented 2008 feb 14]

Specific heat increases with temperature for geologic materials and martian conditions. Theoretical models range from the classic model of Debye to the comprehensive formulation of S.W Kieffer SWKieffer79=[36]. There are several few-term emperical relations , e.g. $\frac{A}{B+T}$, $\left(\frac{T}{T_c}\right)^{\beta}$, polynomial in $\frac{T-T_c}{T_c}$ Ledlow92=[37], $c_1 - c_2/\sqrt{T} - c_3 T^{-2} + c_4 T^{-3}$ where all coefficients are positive Berman85=[11], and others in Waples04=[64]. However, it was found that over the full range of martian temperatures a cubic polynomial would fit geologic materials with error $< 1\%$. A temperature-scaled polynomial of the same form as for thermal conductivity has been implimented [2010 feb].

The layer setup described in the prior section remains based on the values of the physical properites at a reference temperature, chosen to be 220 K, which is the approximate midpoint of the full range of surface temperatures on Mars.

Compute once per run: $F_{C_i} = \frac{2\Delta t_i}{\rho_i B_i^2}$ and $F_{B_i} = B_+/B_i$

Compute once per time step: $F_{k_i} = k_i/k_+$

Then Equations 20 and 22 become

$$F_{1_i} = F_{C_i} \cdot \frac{k_i / C_P(T)}{1 + F_{B_i} F_{k_i}} \qquad \text{eq : F1t} \tag{24}$$

and

$$F_{3_i} = \frac{1 + F_{B_i} F_{k_i}}{1 + 1/\left(F_{k_-} F_{B_-}\right)}. \qquad \text{eq : F3t} \tag{25}$$

Eq. 22 remains the same, but must be evaluated for every layer and time-step.

3.2.2 Solving the upper boundary condition

When there is no surface frost, the net energy into the upper boundary must be zero. From Eq. 13, find

$$\frac{\partial W}{\partial T} = -k/X_2 - 4\Omega\epsilon\sigma T^3 \tag{26}$$

Note that this assumes that the temperature gradient in top half of layer 2 is linear. If KofT, then k is approximated as that of the top material layer at the end of the prior time-step.

The surface kinetic temperature for a balanced boundary condition, Eq. 13, is iterated with Newton convergence until the change in T, $\delta \equiv \frac{W}{\partial W/\partial T}$, is $<$ GGT

If $\mid \delta \mid /T > 0.8$, it is assumed that the model has gone unstable and it is terminated.
if $\mid \delta \mid /T > 0.1$, then δ is reduced by 70% before the next iteration to improve stability

If frost is present, the unbalanced energy W is applied to condensation or sublimation.

After determining the surface temperature, the virtual layer ($i = 1$) temperature is set to yield the proper heat flow between the surface and the top physical layer ($i = 2$);

$$T_1 = T' - (T_2 - T')\frac{B_1\kappa_2}{B_2\kappa_1} \qquad \text{OR} \qquad T_1 = T_2 - (1 + 1/\texttt{RLAY}')\,(T_2 - T') \tag{27}$$

3.2.3 Stability and Binary time expansion

The classic convergence stability criterion is $\frac{\Delta t}{(\Delta Z)^2}\kappa < \frac{1}{2}$, equivalent to $B^2 > 2\Delta t\kappa$. A convergence safety factor is defined as $B_i/\sqrt{2\Delta t_i \cdot \kappa_i}$. The process was found to be numerically unstable if this factor is less than about 0.8. The routine will stop with an error message if the safety factor is anywhere less than one. As the layer thickness increases with depth, the routine will repeatedly double the time interval if all the following conditions are met:

The safety factor is larger than 2
The layer is at least the 3rd down
The remaining time intervals are divisible by 2
No more than MAXBOT time doublings will be done

To handle potential large jumps in diffusivity that are allowed between two materials, an initial calculation of the convergence factor for the upper layer of the lower material is made without time-doubling. If this is < 1, then the thickness of this and all lower layers is increased to be just stable. If this factor is greater than the input safety factor, then the number of allowed time-doubling in the upper material is set accordingly.

The numerous input parameters that control the time-depth grid and convergence are based upon extensive testing done during the code development.

3.2.4 Starting conditions

For the first season, the model starts at 18 Hours with the surface temperature normally set to the equilibrium surface temperature of a perfect conductor as calculated in Eq. 11. The bottom temperature is also normally set to this value. The input parameter IB allows the option of setting the initial bottom temperature to TDEEP or also the surface temperature to this value; the latter case is useful for studying details of the disappearance of seasonal frost.

Once the top and bottom temperatures are set, all intermediate layer temperatures are set by linear interpolation with depth. The initial atmosphere temperature is always set to the equilibrium values using Eq. 12.

A second-degree perturbation is applied at the end of the (third) day; this jumps the mean temperature of all layers and the lower boundary to equal the mean surface temperature.

3.2.5 Jump perturbations

A logical flag `LRESET` is normally false. It is set True on day NRSET or later of the first season if the lower boundary is adiabatic, but never on the last day of calculation in a season.

On a day when `LRESET` is true, the summation for average layer temperatures is restarted. At the end of that day, all layer temperatures are offset by $\langle T_s \rangle - \langle T_i \rangle$ so as to yield no net heat flow.

There is an option to instead perturb temperatures based on a linear plus fractional quadratic function of depth between the diurnal average surface and diurnal average bottom temperatures: if DRSET is not zero, then the layer temperature offsets are, using $x = z_i/z_n$ where $_n$ is the bottom layer:

$$\Delta T_i = (\langle T_s \rangle - \langle T_n \rangle)\,(x + \mathrm{DRSET} \cdot x(1-x))$$

3.2.6 Convergence criteria and parameters

At each time step, if there is not frost, the surface boundary equation is iterated until the change in surface temperature is less than GGT.

The test for continuing full computations each day into a season is based upon Δ_T, defined as the RMS change of layer temperatures, including the virtual layer, from the prior day; this is stored at the end of each day in `DTMJ`

The test for making the next day the last is: either the temperature change over the last two days is nearly constant, or the temperature change is small; i.e.:

$$\mid 1 - \frac{\Delta_T}{\Delta_{T,j-1}} \mid \leq \mathsf{DDT} \qquad \text{or} \qquad \Delta_T \leq \mathsf{DTMAX}$$

where $\Delta_{T,j-1}$ is forced to be at least 10^{-6} . Normally, DDT = 0.002, GGT = 0.1 and DTMAX = 0.1

After computation of the last day, there is a final check that convergence has continued: the temperature change has decreased or it is still small; i.e.:

$$\Delta_T \leq \Delta_{T,j-1} \qquad \text{or} \qquad \Delta_T \leq \mathsf{DTMAX}$$

If these tests fail, and there are days left in the season, then daily calculations are resumed.

3.2.7 Prediction to next season

Calculations run from midnight to midnight. When convergence has been reached, commonly in fewer days than separate seasons, the results at the last 3 midnights, y_1, y_2, y_3, are used to forecast asymptotically the model result at the end of the season, $y = b_0 + b_1 r^x$ where x is the number of sols remaining in the season. Normally, this will use a fit over the last 3 midnights; for convenience reformulated as

$$y = y_3 + c_1((1. - r^x) \qquad \mathrm{eq : pred} \tag{28}$$

where $r = \frac{y_3 - y_2}{y_2 - y_1}$ is the ratio of the last two changes, and $c_1 = \frac{y_3 - y_2}{1/r - 1}$. If the fit is not asymptotic (e.g., if $r \geq 1$), or if the forecast distance (from the last computed midnight) is less than 0.9 sols, the routine will do a linear prediction using the most recent two points. In addition, lower and upper limits can be specified, e.g.., to keep a temperature from falling below a frost point.

3.3 Comparison to other thermal models

3.3.1 Comparison to Ames GCM

A specific test case was chosen for comparison of the KRC one-layer atmosphere with the multi-layer radiative, conductive and convective coupled atmosphere of a full Global Circulation Model (GCM), [30]; the Viking-1 landing site, Latitude 22°N, elevation -3.1 km, $L_s = 100°$, $\tau = 0.3$, visible/IR opacity ratio 1.0, surface pressure of 7 millibar, bolometric albedo of 0.25, thermal inertia 270 $\mathrm{J\,m^{-2}s^{-1/2}K^{-1}}$, with a run-up time of 20 sols. The comparison with KRC run with the same conditions is shown in Figures 1 and 2; except that the base KRC model used a ratio of thermal/solar opacity=1.0.

The Ames GCM was run for the same conditions (output data kindly provided by Robert Haberle). Both models were "spun up" for 20 days, the GCM model used a infrared/solar opacity ratio of 1.0 whereas KRC used 0.5.

The GCM surface temperatures are lower than KRC, the most at night. This results largely from having a deep sub-surface model and starting all layers too cold for this season.

The resulting temperatures for $L_s = 100°$ are shown in Fig. 4. The down-going radiation fluxes at the surface for both models are shown in Fig. 5

The atmospheric temperature for the GCM is a layer average weighted by mass. The KRC and GCM atmospheric temperatures have similar phase, with minima near 8H and maxima near 17H, however, the KRC down-going infrared radiance lags the GCM slightly, as expected because the GCM near-surface atmospheric layers dominate the down-going flux and track the surface temperature more closely than the KRC one-layer atmosphere.

The KRC atmosphere down-going infrared radiances are similar to the GCM if the ID/solar opacity ratio is 0.5.

Variations on the KRC model were run to simulate the effect of having a deep model and starting at 180K for a 20 day run, as did the GCM run; these yield surface temperatures about 3 K cooler than a realistic subsurface temperatures.

The GCM used an initial "run-up" of 20 sols and inhibited lateral atmospheric dynamics. KRC used a 3 year start-up (spaced 1/40'th of Martian year) followed by a 20-sol run-up every sol and ; the latter is more realistic for sub-surface conditions and raises all temperatures about 2 K.

3.3.2 Comparison to Mellon model

For TES standard processing, Mellon models were generated at 8 sol intervals and 5°latitude spacing for 10 thermal inertia's spaced logarithmically; for 3 sets of albedo, dust opacity, and average surface pressure. KRC models were generated on the same grid, except only latitudes 85,60,30 and 0, both N and S and for the middle value of albedo (0.25), dust opacity (0.5), and average surface pressure (600 Pa). The same values were used for all physical parameters identified in the Mellon models. The diurnal surface temperature curves for three thermal inertia and three latitudes are shown in Figure 6. KRC models are a few degrees warmer, the greatest at night and for low thermal inertia. A seasonal comparison of is shown in Figure 7; The models track each other closely except for the lowest inertia at 30S near $L_s = 90°$, when CO_2frost forms at night [?? investigate].

3.3.3 Comparison to Vasavada model

Ashwin Vasavada has a model used at JPL for martian surface environments. It incorporates temperature-dependent heat capacity and has the ability to model sloped surfaces. The subsurface portion is based Vasa99=[63] and the atmosphere interaction is based on a 1-D version of the radiative transfer and boundary layer physics from the GFDL Mars GCM, circa 2004 Wilson96,Richardson02,Basu04=[66, 52, 9] and includes basic CO_2 condensation. There is no geothermal heat flux.

A comparison with KRC was done for Holden Crater, a candidate landing site. $k(T)$ was not used. The thermal emissivity is 0.98. The model assumes a constant 10 m/s wind for the boundary layer. After a few years of spin-up and equilibration, the model output values at 15 min time-steps for a martian year (resolving diurnal and seasonal thermal effects in the subsurface). Comparisons are shown for one season in Figure 9.

4 Architecture

The main program can run one or more "cases", which are normally independent except for retaining the input parameters that are not explicitly changed. However, "linking" runs that transfer forward the current conditions (layer temperatures, frost budget, atmospheric temperature) is possible; see Section 4.9.

The main program, **KRC** calls **TDAY,1** once with a flag that precomputes everything possible about the subsurface numerical scheme, and then for each season calls:

TSEAS which determine the distance and declination of the Sun, and then calls

TLATS which loops over latitudes, calculating insolation and atmospheric parameters for one latitude and calling

TDAY,2 which does the layer calculations for each time step and each "day" needed to reach convergence.

In addition to the FORTRAN version, IDL interfaces to KRC exist.

4.1 Main program, KRC

KRC explicitly sets all common areas to zero (not necessary on most modern computers), defines all logical units, sets physical constants, and asks for the input file name and the output log file name. It calls **TCARD,1** to read the input file up to before the first potential change card.

If **TCARD** reports having detected the one-point mode; the 1-point flag is set in common so all routines will know, the initial input file is closed, and the input list of points and the output table file are opened. **TCARD,2** is called to get the first 1-point.

KRC now starts a case and calls **TSEAS**. The remainder of **KRC** is logic and looping control for seasons or 1-points, additional cases and control of optional printing and binary output files.

4.2 Input: TCARD

All input other than the initial two file names is handled by one routine, **TCARD**, which reads lines from the input file[s]. The first integer on a card controls the action to be taken, there are 12 possibilities, described in *helplist.tex*, which allow changing all integer, real, logical input parameters, the latitude set, the elevations set, titles and file names, and 1-point sets. It also tests for formal errors on array sizes, loop limits and some physical constants. A sample input file is shown in Appendix A

g

4.3 Seasons: TSEAS

This routine initializes or increments the season counter and computes the current Modified Julian Date (offset from 2,440,000). If LSC true (rare), it calls **TCARD,2** to read any parameter changes and then **TDAY,1** to set up the subsurface model. The Sun-planet geometry is obtained from **PORB** [Planet ORBit] and the L_s computed; the same geometry is used throughout a "season". Notification of execution time thus far will be sent to the terminal if LNOTIF is True and the season count is a multiple of NMOD.

If SVALB if True, then at each season the soil albedo will be derived by linear interpolation in L_s of the albedo table. A similar seasonal variation for atmospheric opacity is available by setting SVTAU True.

The routine **TLATS** is called to do calculations for all latitudes, after which there are options to print a diurnal surface temperature table and layer minimum/maximum temperature table by calling the routine **TPRINT**, which handles nearly all printout.

For certain kinds of binary output (K4OUT < 0) and if the season counter is JDISK and if the run is not a continuation from a prior file, then **TDISK,5** is called to write the Common area KRCCOM to disk. if K4OUT is not zero, for every season starting with JDISK, the results for that season are written to the binary output file.

4.4 Latitude calculations: TLATS

TLATS is called once per season. Using solar geometry information in Common, it calculates insolation-related values that are constant across latitude. It sets the reference-level surface pressure as described in §2.4.2; if based on polar cap mass, then the routine **TINT** is called to do the global integration; there is an option for **TPRINT,8** to print the global properties.

Looping over latitude, the local surface pressure is calculated. The solar radiation absorbed at the surface and in the atmosphere are calculated for every time-of-day step, including consideration of insolation-dependent frost albedo if that was specified. There is an option to print the values for each hour. The equilibrium temperature conditions are computed; and starting conditions are set to the ending conditions for the prior season, if any.

The routine **TDAY,2** is called to do the diurnal calculations for one latitude. Based on the number of sols required to reach convergence, temperatures at midnight for all layers, the surface, the bottom, and the atmosphere, along with the amount of frost, are predicted to the end of the season; see §3.2.7. There are options to print a convergence summary and hourly radiation conditions.

4.5 Diurnal calculations: TDAY

The routine **TDAY** continues the inner loops for depth, time of day, and days to convergence; most of the execution time is in this routine. It is coded to minimize the computation time. There are two major sections; **TDAY,1** sets up the subsurface layer and time grid, checking for stability. It computes and saves values that are independent of surface conditions. **TDAY,2** solves the boundary conditions and the diffusion equation, including atmospheric temperature.

TDAY,2 has an outer loop for days-to-convergence; this resets some summations and for the last day and sets the time steps for print and disk output. A middle loop runs over time-of-day; it interpolates the upper two layers to the surface temperature, implements the lower boundary condition, and sets the number of layers to be used for this time step.

There are two inner loops to solve the diffusion equation, they have a total of 10 indexing (two with fixed offsets) and five floating point operations per layer.

After the inner loops, the middle loop finds the new surface heat flow, solves the boundary conditions, computes the new atmospheric temperature and checks for saturation, and modifies any frost amount. If frost appears new or disappears entirely, the frost flag is set appropriately and surface albedo and emissivity reset. If the current day is the last to be computed this season, and the time is on an hour, then hourly conditions are saved and printed.

In the outer loop, midnight conditions and daily averages are saved. Convergence conditions and iteration counts are checked to see if a jump should be done or if the next day can be the last or if the routine is finished.

4.6 Disk Output: TDISK

TDISK handles all binary input/output. It can write a variety of contents for each season. These have been developed over time to address various research issues. Planetary temperature is that defined in Eq. 8.

Direct access files: a record for each season

-1 KRCCOM plus LATCOM. Only this version supports restarting from a specific season.

0 one record of KRCCOM, latitudes and elevations; then records each season for of hourly surface kinetic and planetary brightness temperatures for every latitude

1:49 KRCCOM and DAYCOM for the last latitude.

One large array for all seasons, latitudes and cases, with KRCCOM loaded into a "virtual" part of the array. The number of cases depends upon number of layers, latitudes and seasons, and is described in *helplist.tex*.

51 Surface and planetary temperatures for every hour, latitude and season. Plus, for every season, the date, L_s, PZREF, dust opacity and total frost.

52 For each latitude, surface, planetary and atmosphere hourly temperature and diurnal layer extremes and NDJ4, DTM4, TTA4, FROST4, AFRO4, HEATMM. Plus, for every season, the date, L_s, PZREF, dust opacity and total frost.

54 Surface temperature at 1 and 13 Hours, diurnal-average upward heat flow, midnight frost amount and bottom temperature.

55 For one latitude, 10 items related to temperatures, frost and heat-flow. Useful for large number of seasons.

56 Designed for seasonal cap studies; hourly surface and planetary temperatures, plus several parameters at midnight for each latitude, plus several global parameters each season.

4.7 Commons

All commons are contained in separate files that are included into routines at compilation. The primary file contains constants that set the sizes of arrays, and the main Common, **KRCCOM** which contains all input parameters, some physical constants, and all the major loop indices.

LATCOM contains results for latitudes

DAYCOM contains layer temperature extremes and the values at midnight, several conditions at the end of each iteration day, radiation and surface temperature values at each time step, and indices of time-doubling layers.

HATCOM contains arrays related to heat flow and irradiance

UNITS contains logical unit assignments, open/closed flags and error message indices.

FILCOM contains all file names

PORBCM contains planetary geometry and rotation matrices

4.8 Print file

Tprint output; Describe each flag

Describe print options

Sample layer table

4.9 Linked Runs

Seasonal details by continuing with 1-day season

KRC has the ability to continue from the vertical temperature profile at the end of a prior case, as long as the physical distribution of the layers is not changed.

By continuing from memory and incrementing the total number of seasons, it is possible to continuously change parameters such as the atmospheric opacity.

4.9.1 Routine when2start

If a specific season is desired, an IDL routine is available to compute the proper initial date.

```
function when2start, ls,j5,del
;_Titl WHEN2START Calc starting date for KRC to reach Ls on specific season step
; ls    in.     Float.  L_sub_S target
; j5    in.     Integer. Step on which to reach target
; del   in.     Float. KRC season step size OR negative  of either:
;               number of Sols. <36 OR intervals per Mars-years >35
```

This can be used multiple times for linked runs. For example, to "spin up" for 3 Mars' years of 40 seasons each, then run daily for 20 sols and end at $L_s = 100°$, call in reverse order; because this routine treats indices as 1-based, if second date-interval set adds N intervals, use N+1 as target index.

print, when2start(100.,21,1.0275)

Will print a starting date of 11896.82, at which time $L_s = 90.86$

print, when2start(90.86,120,17.1745)

will print the needed starting date of 9853.04

4.10 One-point version (an alternate input)

To support the THEMIS team, an interface to the KRC system was built that computes the temperature for a single condition. The user generates a file 'one.inp' that contains lines of specific times and conditions.

The input file *Mone.inp* is set to do one latitude for 2 seasons. All the iteration and convergence parameters can be set in this file to achieve the accuracy desired. The input file contains a change-card 10 which points to 'one.inp' as the file of specific points.

4.10.1 Guide to running in one-point mode

A parameter initialization file Mone.inp is provided. It sets the KRC system into a reasonable mode for one-point calculations.

A line near the end of that file points to a file 'one.inp' which can contain any number of one-point conditions. 'one.inp' is intended to be edited to contain the cases desired; however, it must maintain the input format of the sample file.

First line is a title, which can be changed freely. The second line is an alignment guide for the location lines and should not be modified; both these lines must be present.

Each following line must start with an '11 '; this is a code that tells the full-up KRC that this is a one-point line. The next 9 fields are read with a fixed format, and each item should be aligned with the last character of the Column title. All items must be present, each line must extend at least to the m in Azim; comments may extend beyond that, but they will not appear in the output file. Be sure to have a ¡CR¿ at the end of the last input line.

The fields (after the 11) in the one-point input are:

Ls L_S season, in degrees
Lat Aerographic latitude in degrees
Hour Local time, in 1/24'ths of a Martian Day
Elev Surface elevation (relative to a mean surface Geoid), in Km
Alb Bolometric Albedo, dimensionless
Inerti Thermal Inertia, in SI units
Opac Atmospheric dust opacity in the Solar wavelength region
Slop Regional slope, in degrees from horizontal
Azim Azimuth of the down-slope direction, Degrees East of North.

The two additional columns in the output file are:

TkSur Surface kinetic temperature
TbPla Planetary bolometric brightness temperature

—– Comments on the One-point model.

The initialization file of 2002mar08 is set to compute the temperatures at the season requested without seasonal memory. It uses layers that extend to 5 diurnal skin depths. It does not treat the seasonal frost properly, so don't believe the results near the edge of the polar cap. Execution time on a circa 2001 PC may be the order of 0.01 seconds per case.

The underlying model is the full version of KRC. By modifying the initialization file, you can compute almost anything you might want. If you choose to try this, best to read the remainder of this document.

5 Use

Users guide available in *helplist.tex*; see supporting material. For normal runs, the user will be prompted for the name of the input file and the names of a print file. All actions are controled by the input file.

5.1 Symbols and variables

In Table 1; computation frequency is indicated as:

C = Input constant
F = Firm-coded constant
O = Once
S = Every "season" (may be as frequent as each sol)
H = Every "Hour" (24 times per sol)
R = Rapid: every time-step (Nominal is 384 times per sol)
SR = every time step for one day each season

subscript [f] means that frost values are used if frost is present.
'MARS' indicates that the values were taken from reference [33] at the listed page.

6 Sample Applications and execution time

Polar cap edge and global pressure

nyear @ 1/40 + last year at 1/sol

Redo the Viking models: 19 latitudes, 25 layers, 120 seasons, 3 cases; execution time on a circa 2007 PC was 3.5 seconds.

THEMIS image: 1 lat, 1 season, 8 azimuths, 4 slopes, 5 elevations

Grid interpolation possibilities

References

[1] R. Arvidson, D. Adams, G. Bonfiglio, P. Christensen, S. Cull, M. Golombek, J. Guinn, E. Guinness, T. Heet, R. Kirk, A. Knudson, M. Malin, M. Mellon, A. McEwen, A. Mushkin, T. Parker, F. Seelos, K. Seelos, P. Smith, D. Spencer, T. Stein, and L. Tamppari. Mars Exploration Program 2007 Phoenix landing site selection and characteristics. *Journal of Geophysical Research (Planets)*, 113(E12):0–+, June 2008.

[2] R. E. Arvidson, R. C. Anderson, P. Bartlett, J. F. Bell, D. Blaney, P. R. Christensen, P. Chu, L. Crumpler, K. Davis, B. L. Ehlmann, R. Fergason, M. P. Golombek, S. Gorevan, J. A. Grant, R. Greeley, E. A. Guinness, A. F. C. Haldemann, K. Herkenhoff, J. Johnson, G. Landis, R. Li, R. Lindemann, H. McSween, D. W. Ming, T. Myrick, L. Richter, F. P. Seelos, S. W. Squyres, R. J. Sullivan, A. Wang, and J. Wilson. Localization and Physical Properties Experiments Conducted by Spirit at Gusev Crater. *Science*, 305:821–824, August 2004.

[3] R. E. Arvidson, F. Poulet, R. V. Morris, J.-P. Bibring, J. F. Bell, S. W. Squyres, P. R. Christensen, G. Bellucci, B. Gondet, B. L. Ehlmann, W. H. Farrand, R. L. Fergason, M. Golombek, J. L. Griffes, J. Grotzinger, E. A. Guinness, K. E. Herkenhoff, J. R. Johnson, G. Klingelhöfer, Y. Langevin, D. Ming, K. Seelos, R. J. Sullivan, J. G. Ward, S. M. Wiseman, and M. Wolff. Nature and origin of the hematite-bearing plains of Terra Meridiani based on analyses of orbital and Mars Exploration rover data sets. *J. Geophys. Res. (Planets)*, 111(E10):12–+, November 2006.

[4] H. H. Aumann and H. H. Kieffer. Determination of particle sizes in Saturn's rings from their eclipse cooling and heating curves. *Astron. Jour.*, 183:305–311, 1973.

[5] J. L. Bandfield. High-resolution subsurface water-ice distributions on Mars. *Nature*, 447:64–67, May 2007.

[6] J. L. Bandfield and C. S. Edwards. Derivation of martian surface slope characteristics from directional thermal infrared radiometry. *Icarus*, 193:139–157, January 2008.

[7] J. L. Bandfield and W. C. Feldman. Martian high latitude permafrost depth and surface cover thermal inertia distributions. *J. Geophys.Res.(Planets)*, 113(E12):8001–+, August 2008.

[8] J. R. Barnes, J. B. Pollack, R. M. Haberle, C. B. Leovy, R. W. Zurek, H. Lee, and J. Schaeffer. Mars atmospheric dynamics as simulated by the NASA AMES General Circulation Model. II - Transient baroclinic eddies. *J. Geophys. Res.*, 98:3125–3148, February 1993.

[9] S. Basu, M. I. Richardson, and R. J. Wilson. Simulation of the Martian dust cycle with the GFDL Mars GCM. *J. Geophys. Res. (Planets)*, 109(E18):11006–+, November 2004.

[10] J.F. Bell. *The Martian Surface: Composition, Mineralogy , and Physical Properties.* Cambridge University Press, 2008.

[11] R. G. Berman and T. H. Brown. Heat capacity of minerals in the system Na_2O-K_2O-CaO-MgO-FeO-Fe_2O_3-Al_2O_3-SiO_2-TiO_2-H_2O-CO_2: representation, estimation, and high temperature extrapolation. *Contributions to Mineralogy and Petrology*, 89:168–183, April 1985.

[12] P. R. Christensen, J. L. Bandfield, J. F. Bell, N. Gorelick, V. E. Hamilton, A. Ivanov, B. M. Jakosky, H. H. Kieffer, M. D. Lane, M. C. Malin, T. McConnochie, A. S. McEwen, H. Y. McSween, G. L. Mehall, J. E. Moersch, K. H. Nealson, J. W. Rice, M. I. Richardson, S. W. Ruff, M. D. Smith, T. N. Titus, and M. B. Wyatt. Morphology and composition of the surface of Mars: Mars Odyssey THEMIS results. *Science*, 300:2056–2061, 2003.

[13] P. R. Christensen, H. Y. McSween, J. L. Bandfield, S. W. Ruff, A. D. Rogers, V. E. Hamilton, N. Gorelick, M. B. Wyatt, B. M. Jakosky, H. H. Kieffer, M. C. Malin, and J. E. Moersch. Evidence for magmatic evolution and diversity on Mars from infrared observations. *Nature*, 436:504–509, July 2005.

[14] P. R. Christensen, S. W. Ruff, R. Fergason, N. Gorelick, B. M. Jakosky, M. D. Lane, A. S. McEwen, H. Y. McSween, G. L. Mehall, K. Milam, J. E. Moersch, S. M. Pelkey, A. D. Rogers, and M. B. Wyatt. Mars Exploration Rover candidate landing sites as viewed by THEMIS. *Icarus*, 176:12–43, July 2005.

[15] P. R. Christensen, S. W. Ruff, R. L. Fergason, A. T. Knudson, S. Anwar, R. E. Arvidson, J. L. Bandfield, D. L. Blaney, C. Budney, W. M. Calvin, T. D. Glotch, M. P. Golombek, N. Gorelick, T. G. Graff, V. E. Hamilton, A. Hayes, J. R. Johnson, H. Y. McSween, G. L. Mehall, L. K. Mehall, J. E. Moersch, R. V. Morris, A. D. Rogers, M. D. Smith, S. W. Squyres, M. J. Wolff, and M. B. Wyatt. Initial Results from the Mini-TES Experiment in Gusev Crater from the Spirit Rover. *Science*, 305:837–842, August 2004.

[16] S. M. Clifford and C. J. Bartels. The Mars Thermal Model (marstherm): a FORTRAN 77 Finite-Difference Program Designed for General Distribution. In *Lunar and Planetary Institute Conference Abstracts*, pages 142–143, March 1986.

[17] K. S. Edgett and P. R. Christensen. The particle size of Martian aeolian dunes. *J. Geophys. Res*, 96:22765–+, December 1991.

[18] W. C. Feldman, M. C. Bourke, R. C. Elphic, S. Maurice, J. Bandfield, T. H. Prettyman, B. Diez, and D. J. Lawrence. Hydrogen content of sand dunes within Olympia Undae. *Icarus*, 196:422–432, August 2008.

[19] R. L. Fergason, P. R. Christensen, J. F. Bell, M. P. Golombek, K. E. Herkenhoff, and H. H. Kieffer. Physical properties of the Mars Exploration Rover landing sites as inferred from Mini-TES-derived thermal inertia. *Journal of Geophysical Research (Planets)*, 111(E10):2–+, February 2006.

[20] R. L. Fergason, P. R. Christensen, and H. H. Kieffer. High resolution thermal inertia derived from THEMIS: thermal model and applications. *J. Geophys.Res (Planets)*, 111:E12004, 2006.

[21] I. Gatley, H. H. Kieffer, E. Miner, and G. Neugebauer. Infrared observations of Phobos from Mariner 9. *Astrophys. Jour.*, 190:497–503, 1974.

[22] T. D. Glotch and P. R. Christensen. Geologic and mineralogic mapping of Aram Chaos: Evidence for a water-rich history. *J. Geophys. Res.(Planets)*, 110(E9):9006–+, September 2005.

[23] M. P. Golombek, R. E. Arvidson, J. F. Bell, P. R. Christensen, J. A. Crisp, L. S. Crumpler, B. L. Ehlmann, R. L. Fergason, J. A. Grant, R. Greeley, A. F. C. Haldemann, D. M. Kass, T. J. Parker, J. T. Schofield, S. W. Squyres, and R. W. Zurek. Assessment of Mars Exploration Rover landing site predictions. *Nature*, 436:44–48, July 2005.

[24] M. P. Golombek, R. A. Cook, T. Economou, W. M. Folkner, A. F. C. Haldemann, P. H. Kallemeyn, J. M. Knudsen, R. M. Manning, H. J. Moore, T. J. Parker, R. Rieder, J. T. Schofield, P. H. Smith, and R. M. Vaughan. Overview of the Mars Pathfinder Mission and Assessment of Landing Site Predictions. *Science*, 278:1743–+, December 1997.

[25] M. P. Golombek, R. A. Cook, H. J. Moore, and T. J. Parker. Selection of the Mars Pathfinder landing site. *J. Geophys. Res.(Planets)*, 102:3967–3988, February 1997.

[26] M. P. Golombek, L. S. Crumpler, J. A. Grant, R. Greeley, N. A. Cabrol, T. J. Parker, J. W. Rice, J. G. Ward, R. E. Arvidson, J. E. Moersch, R. L. Fergason, P. R. Christensen, A. Castaño, R. Castaño, A. F. C. Haldemann, R. Li, J. F. Bell, and S. W. Squyres. Geology of the Gusev cratered plains from the Spirit rover transverse. *J. Geophys. Res. (Planets)*, 111(E10):2–+, January 2006.

[27] M. P. Golombek, J. A. Grant, T. J. Parker, D. M. Kass, J. A. Crisp, S. W. Squyres, A. F. C. Haldemann, M. Adler, W. J. Lee, N. T. Bridges, R. E. Arvidson, M. H. Carr, R. L. Kirk, P. C. Knocke, R. B. Roncoli, C. M. Weitz, J. T. Schofield, R. W. Zurek, P. R. Christensen, R. L. Fergason, F. S. Anderson, and J. W. Rice. Selection of the Mars Exploration Rover landing sites. *J. Geophys. Res.(Planets)*, 108:8072–+, December 2003.

[28] R. Greeley, R. E. Arvidson, P. W. Barlett, D. Blaney, N. A. Cabrol, P. R. Christensen, R. L. Fergason, M. P. Golombek, G. A. Landis, M. T. Lemmon, S. M. McLennan, J. N. Maki, T. Michaels, J. E. Moersch, L. D. V. Neakrase, S. C. R. Rafkin, L. Richter, S. W. Squyres, P. A. de Souza, R. J. Sullivan, S. D. Thompson, and P. L. Whelley. Gusev crater: Wind-related features and processes observed by the Mars Exploration Rover Spirit. *J. Geophys. Res.(Planets)*, 111(E10):2–+, January 2006.

[29] R. M. Haberle and B. M. Jakosky. Atmospheric effects on the remote determination of thermal inertia on Mars. *Icarus*, 90:187–204, 1991.

[30] R. M. Haberle, J. B. Pollack, J. R. Barnes, R. W. Zurek, C. B. Leovy, J. R. Murphy, H. Lee, and J. Schaeffer. Mars atmospheric dynamics as simulated by the NASA AMES General Circulation Model. I - The zonal-mean circulation. *J. Geophys. Res.*, 98:3093–3123, February 1993.

[31] J. H. Joseph, W. J. Wiscombe, and J. A. Weinman. The delta-Eddington approximation for radiative flux transfer. *Journal of Atmospheric Sciences*, 33:2452–2459, 1976.

[32] H. H. Kieffer. Cold jets in the Martian polar caps. *Jour. Geophys. Res., Planets*, 112(E11):8005–+, August 2007.

[33] H. H. Kieffer, B. M. Jakosky, C. W. Snyder, and Eds. M. S. Matthews. *Mars*. University of Arizona Press, Tucson, 1992. 1498 pp.

[34] H. H. Kieffer, T. Z. Martin, A. R. Peterfreund, B. M. Jakosky, E. D. Miner, and F. D. Palluconi. Thermal and albedo mapping of Mars during the Viking primary mission. *J. Geophys. Res.*, 82:4249–4291, 1977.

[35] H. H. Kieffer, T. N. Titus, K. F. Mullins, and P. Christensen. Mars south polar spring and summer behavior observed by TES: Seasonal cap evolution controlled by frost grain size. *J. Geophs. Res.*, 105(E4):9653–9699, 2000.

[36] S. W. Kieffer. Thermodynamics and lattice vibrations of minerals. I - Mineral heat capacities and their relationships to simple lattice vibrational models. II - Vibrational characteristics of silicates. III - Lattice dynamics and an approximation for minerals with application to simple substances and framework silicates. *Reviews of Geophysics and Space Physics*, 17:1–59, February 1979.

[37] M. J. Ledlow, M. Zeilik, J. O. Burns, G. R. Gisler, J.-H. Zhao, and D. N. Baker. Subsurface emissions from Mercury - VLA radio observations at 2 and 6 centimeters. *Astrophys. J.*, 384:640–655, January 1992.

[38] T. Z. Martin. Thermal correction of MRO CRISM data using photoclinometry and slope-dependent thermal models for the Martian surface. In *Bulletin of the American Astronomical Society*, volume 36 of *Bulletin of the American Astronomical Society*, pages 1160–+, November 2004.

[39] M. T. Mellon, B. M. Jakosky, H. H. Kieffer, and P. R. Christensen. High-resolution thermal inertia mapping from the Mars Global Surveyor Thermal Emission Spectrometer. *Icarus*, 148:437–455, December 2000.

[40] S. A. Nowicki and P. R. Christensen. Rock abundance on Mars from the Thermal Emission Spectrometer. *Journal of Geophysical Research (Planets)*, 112(E11):5007–+, May 2007.

[41] M.M. Osterloo, V.E. Hamilton, J.L. Bandfield, T.D. Glotch, A.M. Baldridge, P.R. Christensen, L.L. Tornabene, and F.S. Anderson. Chloride-bearing materials in the Southern highlands of Mars. *Science*, 319:1651, 2008.

[42] D. A. Paige. The annual heat balance of the Martian polar caps from Viking observations. *Ph.D. thesis*, California Inst. of Technology., 1985.

[43] D. A. Paige. The thermal stability of near-surface ground ice on Mars. *Nature*, 356:43–45, 1992.

[44] D. A. Paige, J. E. Bachman, and K. D. Keegan. Thermal and albedo mapping of the polar regions of Mars using Viking thermal mapper observations 1. north polar region. *J. Geophys. Res.*, 99:25,959–25,991, 1994.

[45] D. A. Paige and K. D. Keegan. Thermal and albedo mapping of the polar regions of Mars using Viking thermal mapper observations 2. south polar region. *J. Geophys. Res.*, 99:25,993–26,013, 1994.

[46] D. A. Paige and S. E. Wood. Modeling the Martian seasonal CO_2 cycle. *Icarus*, 99:15–27, 1992.

[47] S. Piqueux and P.R. Christensen. North and south subice gas flow and venting of the seasonal caps of Mars: A major geomorphological agent. *J. Geophys. Res.*, 113:E06005, 2008.

[48] S. Piqueux, C.S. Edwards, and P.R. Christensen. Distribution of the ices exposed near the south pole of Mars using Thermal Emission Imaging System (THEMIS) temperature measurements. *J. Geophys. Res.*, 113:E08014, 2008.

[49] M. A. Presley and P. R. Christensen. Thermal conductivity measurements of particulate materials 2. results. *J. Geophys. Res.*, 102(E3):6551–6566, March 1997.

[50] N. E. Putzig and M. T. Mellon. Apparent thermal inertia and the surface heterogeneity of Mars. *Icarus*, 191:68–94, 2007.

[51] N. E. Putzig, M. T. Mellon, K. A. Kretke, and R. E. Arvidson. Global thermal inertia and surface properties of Mars from the MGS mapping mission. *Icarus*, 173:325–341, February 2005.

[52] M. I. Richardson, R. J. Wilson, and A. V. Rodin. Water ice clouds in the Martian atmosphere: General circulation model experiments with a simple cloud scheme. *J. Geophys. Res. (Planets)*, 107:5064–+, September 2002.

[53] A. D. Rogers, P. R. Christensen, and J. L. Bandfield. Compositional heterogeneity of the ancient Martian crust: Analysis of Ares Vallis bedrock with THEMIS and TES data. *Journal of Geophysical Research (Planets)*, 110(E9):5010–+, May 2005.

[54] S. W. Ruff, P. R. Christensen, R. N. Clark, H. H. Kieffer, M. C. Malin, J. L. Bandfield, B. M. Jakosky, M. D. Lane, M. T. Mellon, and M. A. Presley. Mars' "White Rock" feature lacks evidence of an aqueous origin: Results from Mars Global Surveyor. *Jour. Geophys. Res.*, 106(15):23921–23928, October 2001.

[55] K. P. Seidelmann, editor. *Explanatory Supplement to the Astronomical Almanac*. University Science Books, Mill Valley, California, 2005.

[56] P. K. Seidelmann, B. A. Archinal, M. F. A'Hearn, D. P. Cruikshank, J. L. Hilton, H. U. Keller, J. Oberst, J. L. Simon, P. Stooke, D. J. Tholen, and P. C. Thomas. Report of the IAU/IAG Working Group on Cartographic Coordinates and Rotational Elements: 2003. *Celestial Mechanics and Dynamical Astronomy*, 91:203–215, March 2005.

[57] P. K. Seidelmann, L. E. Doggett, and M. R. Deluccia. Mean elements of the principal planets. *Astron. Jour.*, 79:57–+, January 1974.

[58] E. P. Shettle and J. A. Weinman. The Transfer of Solar Irradiance Through Inhomogeneous Turbid Atmospheres Evaluated by Eddington's Approximation. *Journal of Atmospheric Sciences*, 27:1048–1055, October 1970.

[59] M. D. Smith. Interannual variability in TES atmospheric observations of Mars during 1999-2003. *Icarus*, 167:148–165, January 2004.

[60] J. E. Tillman, N. C. Johnson, P. Gettorp, and D. B. Percival. The Martian annual atmospheric pressure cycle: years without great dust storms. *J. Geophys. Res.*, 98:10963–10971, 1993.

[61] T. N. Titus, H. H. Kieffer, and P. N. Christensen. Exposed water ice discovered near the south pole of Mars. *Science*, 299:1048–1051, 2003.

[62] T. N. Titus, H. H. Kieffer, and K. F. Mullins. Slab ice and snow flurries in the Martian polar night. *J. Geophys. Res.*, 106(E10):23,181–23,196, 2001.

[63] A. R. Vasavada, D. A. Paige, and S. E. Wood. Near-Surface Temperatures on Mercury and the Moon and the Stability of Polar Ice Deposits. *Icarus*, 141:179–193, October 1999.

[64] D.W Waples and J.S. Waples. A review and evaluation evaluation of specific heat capacities of rocks, minerals, and subsurface fluids. part 1: Minerals and nonporous rocks. *Natural Resorces Res.*, 13:97–112, June 2004.

[65] P. R. Weissman and H. H. Kieffer. Thermal modeling of cometary nuclei. *Icarus*, 47:302–311, 1981.

[66] R. J. Wilson and K. Hamilton. Comprehensive model simulation of thermal tides in the Martian atmosphere. *J. Atm. Sci.*, 53:1290–1326, May 1996.

A Sample input file for Mars

Below is a typical input file for Mars. All parameter values should be right-aligned with the parameter name above it. The line beginning "08 Sep 29" and the following block of floating-point numbers specifies the planetary spin axis, the orbit, and contains the associated rotation matrices. All lines below that are "change cards" allowing modification of most parameters; each specified by type (the first number; 1=real 2=integer 3=logical, values greater than 3 have special meaning, explained in the Helplist), location within type (the 2'nd number), new value (the 3'rd number) and a comment which will be printed (4'th item). By FORTRAN convention, everything after a "/" is not read, and thus allows notation in this file. A line beginning with a 0 terminates a set of change cards and starts a new KRC "case". A 2'nd consecutive 0 will terminate the program.

It is possible (by setting `LSC` True) to read change cards at each season; this requires care to not change any dimensions.

Input: input.tex

```
 0 0 / KOLD: season to start with;  KEEP: continue saving data in same disk file
Default values for all parameters. 19 latitudes with mean Mars elevation
    ALBEDO     EMISS   INERTIA     COND2     DENS2    PERIOD SPEC_HEAT   DENSITY
       .25      1.00     200.0       3.4     928.0    1.0275      630.     1600.
      CABR       AMW   -ABRPHA    PTOTAL     FANON      TATM     TDEEP   SpHeat2
      0.11      43.5     -0.00     510.0      .055     200.     180.0     1300.
      TAUD     DUSTA    TAURAT     TWILI      ACR2     -ARC3     SLOPE    SLOAZI
       0.3       .90       0.5       0.0       0.5     -0.00       0.0       90.
    TFROST    CFROST    AFROST     FEMIS       AF1       AF2    FROEXT      FD32
     146.0   589944.       .65      0.95      0.54    0.0009      50.       0.0
      RLAY      FLAY     CONVF     DEPTH     DRSET       DDT       GGT     DTMAX
    1.2000     .1800    2.0000       0.0       0.0     .0020       0.1       0.1
```

```
      DJUL    DELJUL  SOLARDEC       DAU      HLON    SOLCON      GRAV    Atm_Cp
   10322.34  17.1745      00.0     1.465        .0     1368.     3.727     735.9
        N1        N2        N3        N4        N5       N24        IB        IC
        20       384        16        19       120        24         0         0
     NRSET      NMHA      NRUN     JDISK     IDOWN       I14       I15     KPREF
         3        24         1        81        -7        45        65         1
     K4OUT     JBARE      NMOD    IDISK2                                    end
        52         0         5         0                                     0
    LP1    LP2    LP3    LP4    LP5    LP6 LPGLOB   LVFA   LVFT  debug
      F      T      F      F      F      F      F      F      F      F
  LPORB   LKEY    LSC LNOTIF  LOCAL   LD16 LPTAVE Prt.78 Prt.79   LONE
      T      F      F      T      T      F      F      F      F      F
LATITUDES: in 10F7.2  _____7 _____7 _____7 _____7 _____7 _____7 _____7
 -87.50 -80.00 -70.00 -60.00 -50.00 -40.00 -30.00 -20.00 -10.00   0.00
  10.00  20.00  30.00  40.00  50.00  60.00  70.00  80.00  87.50  -0.00
Elevations: in 10F7.2 _____7 _____7 _____7 _____7 _____7 _____7 _____7
   3.51   2.01   1.39   1.22   0.38   0.48   1.17   1.67   1.26   0.17
  -0.94  -1.28  -1.99  -2.51  -3.52  -4.08  -4.51  -4.38  -2.57  -0.00
  08 Sep 29 10:41:33 =RUNTIME.  IPLAN AND TC=   4.0 0.55000
   4.000000      0.5500000      0.8650615      0.3229325E-01   5.000821
  0.9340634E-01   1.523671       12882.95       686.9650      0.9229904
   5.544495       24.62280       0.000000      0.4093198       0.000000
   0.000000       0.000000       0.000000       6.159676      0.4662921
  0.4172604E-01  0.6197483       4.381073       0.000000       1.228627
  0.6619807       0.000000       1.391099      0.1075499     -0.3195100E-01
  0.2263214      -1.246176     -0.5861457     -0.8611114E-01  0.8908045
  0.4461527     -0.9063585      0.1158813     -0.4063075     -0.4136413
 -0.4393618      0.7974096      0.9138050     -0.4049719     -0.3095386E-01
  0.4054090      0.9140893      0.9184200E-02  0.2457525E-01 -0.2094154E-01
  0.9994786     -0.3252879     -0.8556869     -0.4024770      0.9456150
 -0.2943530     -0.1384504      0.7823110E-07  0.4256245     -0.9048999
8 0 0 '/work1/krc/mars/master.t52' / Disk file name
1 12 540.  'PTOTAL set to yield 7  mb at VL1 @ Ls=100'
1 35 4. 'CONVF' / push time doubling start deeper
0/
0/
0/
```

End of input: input.tex

Below is an example of an elaborate set of change cards that looks in detail at the temperatures through the first 40 sols of ice freshly exposed at the bottom of a conical pit. It uses 3 latitudes and does 5 cases; the first is ice freshly exposed to a full hemisphere of sky, followed by pits with slopes of 45 and 25 degrees, then these two pits with a different initial ice temperature

```
7 7 7 'Pit dug to ice by Phoenix' / New title
8 0 0 '../output/phx4.t52' / Disk file name/
1  1 .20 'Albedo'
1  3 2025.3 'Inertia for ice' /
1  7 1300.  'Spec heat' / for ice
1  8 928. 'Density' / for ice
1 15 185. 'TDEEP' /
1 17 0.2 'TAUD'
1 39 .001 'GGT: set to avoid ending early' / set for daily output
1 41 11920.2 'DJUL' / starting date
1 42 1.0275 'DELJUL  1 sol' / set for daily output
2  1 19 'Num Layers' /
```

```
2  3 1  'N3: set to run each day' / set for daily output
2  4 3  'N4' / number of latitudes
2  5 40 'N5' /  total number of seasons = sols
2  7 2  'IB start all =TDEEP' /
2 12 1  'JDISK start immediately' /
2 17 52 'K4OUT: 6 items'/  2 17 51 'K4OUT: 30 layers'/
4 77 77 'New Latitudes' / Must be N4 of them in  10F7.2
  65.00  70.00  72.00 -10.00   0.00  10.00  25.00  45.00  70.00  22.00
5 77 77 'New Elevations' / Must be N4 of them in  10F7.2
   -3.5   -3.5   -3.5   00.0   00.0   00.0   00.0   00.0   00.0   -3.1
0/
1 24 -400. 'Azimuth. Set flag to indicate  a pit' /
1 23 45. 'Slope' / slope of pit wall
0/
1 23 65. 'Slope' /
0/
1 23 45. 'Slope' /
1 15 220. ' TDEEP' /
0/
1 23 65. 'Slope' /
0/
0/
0/
```

B Tables

Input: symbols.tex

Table 1: Symbols and variables

Sym -bol	Name in Code	Input File label or Equation	Value+ frequency	Description and basis
A	AS		S,R$_f$	Current bolometric albedo.
c_p	ATMCP	Atm_Cp	860. C	Atm. specific heat at constant pressure. J K^{-1} kg^{-1}, MARS p.855
C_1	CABR	CABR	0.11 C	Clear atmosphere IR absorption.
C_2	TAURAT		0.5 C	IR/vis relative opacity. Viking VIS & IRTM opacities. MARS p.1022,5
F_3	FAC3	$(1-A_{[f]})$	S,R$_f$	Surface solar absorbtance.
F_4	FAC4	$1+1/\mathrm{RLAY}$	O	Layer factor.
F_5	FAC5	$\Omega\epsilon\sigma$	O	Surface thermal emission factor.
$4F_5$	FAC45	$4\Omega\epsilon\sigma$	O	Surface thermal emission factor
F_6	FAC6	$\Omega\epsilon_{[f]}$	O	Surface emission factor.
F_7	FAC7	$\frac{k}{X_2}$	O	Layer scaling.
F_8	FAC8	$e^{-\tau_R}\epsilon_{[f]}$	O	Fraction of surface blackbody reaching top-of-atmosphere.
F_9	FAC9	$\sigma(1-e^{-\tau_e})$	O	
G	GRAV	GRAV	3.727 C	Martian gravity. m s^{-1}
G_H	GO	ARC2	0.5 C	Henyey-Greenstein asymmetry. MARS p.1030
$\mathcal{H}$	SCALEH		S	Scale height in km. Based on TATM*
H_R	ADGR		SR	Solar heating of atm. Wm^{-2}
H_V	ADGR		SR	Solar heating of atm. Wm^{-2}
i			SR	Incidence angle from zenith onto a horizontal surface.
i_2			SR	Incidence angle onto local slope; from SLOPE and SLOAZI
k	COND	COND	C	Thermal conductivity of the soil. Wm^{-1}K^{-1}
M			R$_f$	Columnar mass of CO_2frost kg m^{-2}
$\mathcal{M}$	AMW		43.5 C	Atomic weight of general atmosphere. (g/mole).
P_0	PTOTAL	PTOTAL	689.7 C	Global annual mean surface pressure. Pa
P_g	PZREF		S	Current pressure at reference level. Pa
P	PRES		S	Current local surface pressure. Pa
$R_{\Downarrow t}$	ATMRAD	$F_9T_a^4$	R	Hemispheric emission from a gray slab atmosphere. Wm $^{-2}$
S_o	SOLCON	SOLCON	1368. C	Solar constant. Wm^{-2}
S_M	SOL	S_o/U^2	S	Solar flux at Mars. Wm^{-2}
$S'_{(t)}$	ASOL		SR	Total insolation onto [sloped] surface. Wm^{-2}
T	TSUR		R	Surface kinetic temperature. Kelvin
T_a	TATM	TATM	200. C*	Temperature of the atmosphere. Kelvin
T_a	TATMJ		R	Temperature of the atmosphere. Kelvin
T_P	TPFH		R	Nadir planetary temperature. Kelvin
t			-	Time from midnight. "Hour"
U	DAU		S	Heliocentric range. Astronomical Units
W	POWER		R	Energy into the surface boundary. Wm^{-2} s^{-2}

Computation frequency is indicated as:

C = Input constant
F = Firm-coded constant
O = Once
S = Every "season" (may be as frequent as each sol)
H = Every "Hour" (24 times per sol)
R = Rapid: every time-step (Nominal is 384 times per sol)
SR = every time step for one day each season

subscript $[f]$ means that frost values are used if frost is present.
'MARS' indicates that the values were taken from reference Mars92=[33] at the listed page.

Table 2: Symbols and variables: Continued

Sym -bol	Name in Code	Input File label or Equation	Value+ frequency	Description and basis
α	1-SKYFAC	$(1-\alpha)$	S	Fraction of upper hemisphere occupied by ground = slope/180°
β	BETA	$1-e^{-\tau_R}$	S	Vertical thermal absorption of atmosphere
β_e	BETH	$1-e^{-\tau_e}$	S	Hemispheric thermal absorption of atmosphere
γ	TWILFAC		S	Twilight extension factor = 90/(90+twilight)
δ	[R]SDEC		S	Solar declination.
$\epsilon_{[f]}$	EMIS		S,R$_f$	Surface emissivity. FEMIS for frost
θ	DLAT		S	Latitude. θ_2 = latitude + slope north
μ_0	COSI		R	Cosine of the incidence angle
ϖ	OMEGA	DUSTA	0.9 C	Dust grain single scattering albedo. MARS p.1030
Ω	SKYFAC	$\equiv 1-\alpha$	SR	Fraction of the sky (upper hemisphere) that is visible to the surface
σ	SIGSB	5.67051e-8	F	Stephan-Boltzman constant. W m^{-2} K^{-4}
τ_0	TAUD	TAUD	0.2 C	Nominal solar-range dust opacity
τ	OPACITY		S	Current local dust opacity
τ_e	TAUEFF		S	Effective thermal opacity of the atmosphere
τ_R	TAUIR		S	Thermal opacity, zenith
ϕ	ANGLE		R	Hour angle from midnight, ϕ_2 = hour angle + slope east
$\langle\ \rangle$				diurnally-averaged value
	TWILI	TWILI	1.0 C	Central angle extension of twilight, degrees
	DTAFAC	$\Delta t/(c_p\frac{P}{g})$	O	Atmosphere heating factor. s^{2}m^{2}K W^{-1}
	FEMIT	$\Omega\epsilon_f\sigma T_f^4$	O	Frost thermal emission.

End of input: symbols.tex

Input: layers.tex

End of input: layers.tex

Input: routines.tex

End of input: routines.tex

Table 3: Sample layer table

RUN-CASE 1- 1 05 Nov 19 16:45:41 PAGE= 3

Conductiv.= 3.400E+00 Dens*Cp= 1.206E+06 Diffu.= 2.818E-06 Scale= 2.822E-01

	___THICKNESS____		_______CENTER_DEPTH_____		CONVERGENCE	
LAYER	scale	meter	scale	meter	kg/m^2	factor
1	0.1800	0.0508	-0.0900	-0.0254	0.000	0.000
2	0.2160	0.0610	0.1080	0.0305	56.568	2.851
3	0.2592	0.0731	0.3456	0.0975	124.450	2.053
4	0.3110	0.0878	0.6307	0.1780	205.908	2.956
5	0.3732	0.1053	0.9729	0.2746	303.658	2.129
6	0.4479	0.1264	1.3834	0.3904	420.958	3.065
7	0.5375	0.1517	1.8761	0.5295	561.718	2.207
8	0.6450	0.1820	2.4673	0.6963	730.630	3.178
9	0.7740	0.2184	3.1768	0.8965	933.324	2.288
10	0.9288	0.2621	4.0282	1.1368	1176.557	3.295
11	1.1145	0.3145	5.0498	1.4251	1468.437	2.372
12	1.3374	0.3774	6.2758	1.7711	1818.693	3.416
13	1.6049	0.4529	7.7469	2.1863	2239.000	2.460
14	1.9259	0.5435	9.5123	2.6845	2743.368	3.542
15	2.3111	0.6522	11.6308	3.2823	3348.610	2.550
16	2.7733	0.7826	14.1730	3.9997	4074.901	3.672
17	3.3279	0.9392	17.2236	4.8606	4946.449	5.288
18	3.9935	1.1270	20.8843	5.8937	5992.308	7.615
19	4.7922	1.3524	25.2771	7.1334	7247.337	10.965

Bottom layers for time doubling: 2 4 6 8 10 12 14 19

Table 4: Fortran Code set

Name	description
	Primary routines
KRC	Planet surface thermal model; top routine, MGS-TES version
TSEAS	Advance one "season" along planets orbit
TLATS	Latitude computations
TDAY	Day and layer computations
	Input / output routines
TCARD	Read input file and changes
TDISK	Save/read results at the end of a season; Version with BINF5
TPRINT	Printed output routine
	Specific task routines
ALBVAR	Compute frost albedo as linear function of insolation
ALSUBS	Convert between L_s and days into a Martian year
AVEDAY	Average daily exposure of surface to sunlight.
CO2PT	CO_2 pressure/temperature relation
DEDING2	Delta-Eddington 2-stream solution for single homogeneous layer
EPRED	Exponential Prediction of numerical iteration
TINT	Spherical integrals over globe
VLPRES	Viking lander pressure curves
	Orbit geometry routines
PORB	Computes planetary angles and location for specific time.
PORB0	Planetary orbit. Read pre-computed matrices and do rotation; minimal for KRC
ECCANOM	Iterative solution of Keplers equations for eccentric orbit
ORBIT	Compute radius and coordinates for elliptical orbit
	Utility routines listed in Makefile
Fortran	catime.f datime.f idarch.f sigma.f vaddsp.f xtreme.f binf5.f white1.f
C	b2b.c r2r.c u_move1.c u_move4.c u_swapn.c primio.c pio_bind_c.c
C	binf5_bind.c b_alloc.c b_c2fstr.c b_f2cstr.c b_free.c
	Other routines
IDLKRC	Interface to IDL. Planet surface thermal model MGS-TES version

C Figures

Input: captions.tex

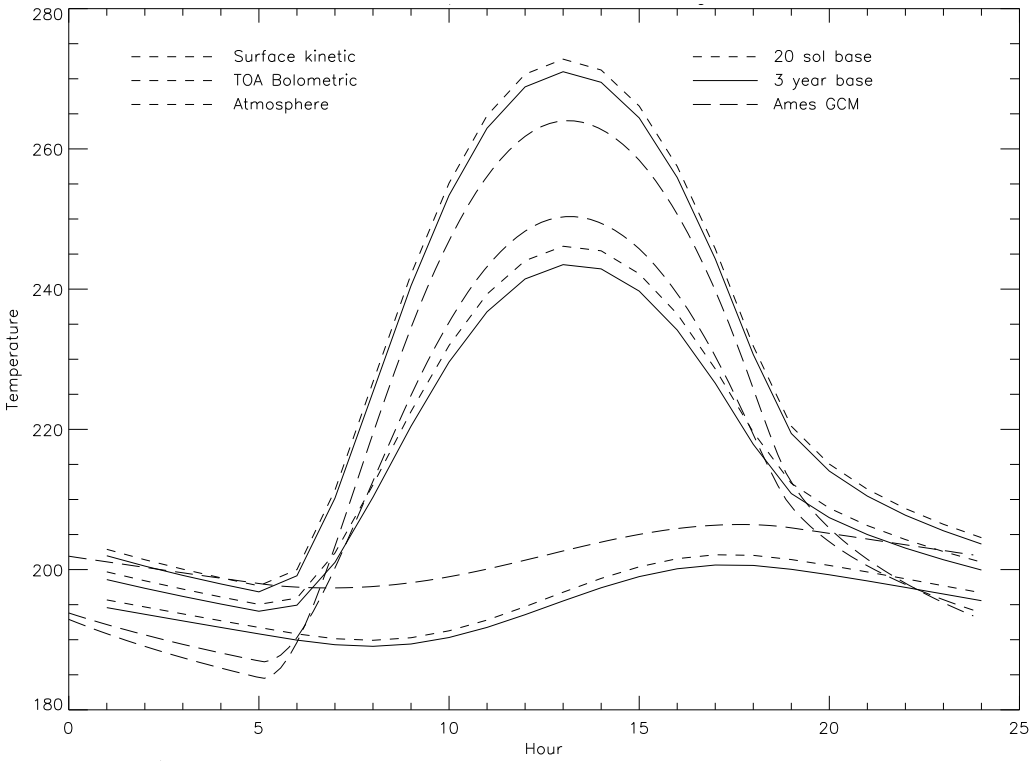

Figure 1: Comparison with GCM results. Calculations for the Viking Lander 1 site at $L_s = 100°$. The input parameter are the same for all models, see text. The upper three lines are surface kinetic temperature through 24 Hours; dashed line is KRC results with a 20-sol run-up, solid line is KRC with a 3 year run-up, and the long-dash line the GCM results with a 20-sol run-up. The lower three curves are the mass-weighted temperature of the atmosphere, and the central three curves are the top-of-atmosphere bolometric temperature.

End of input: captions.tex

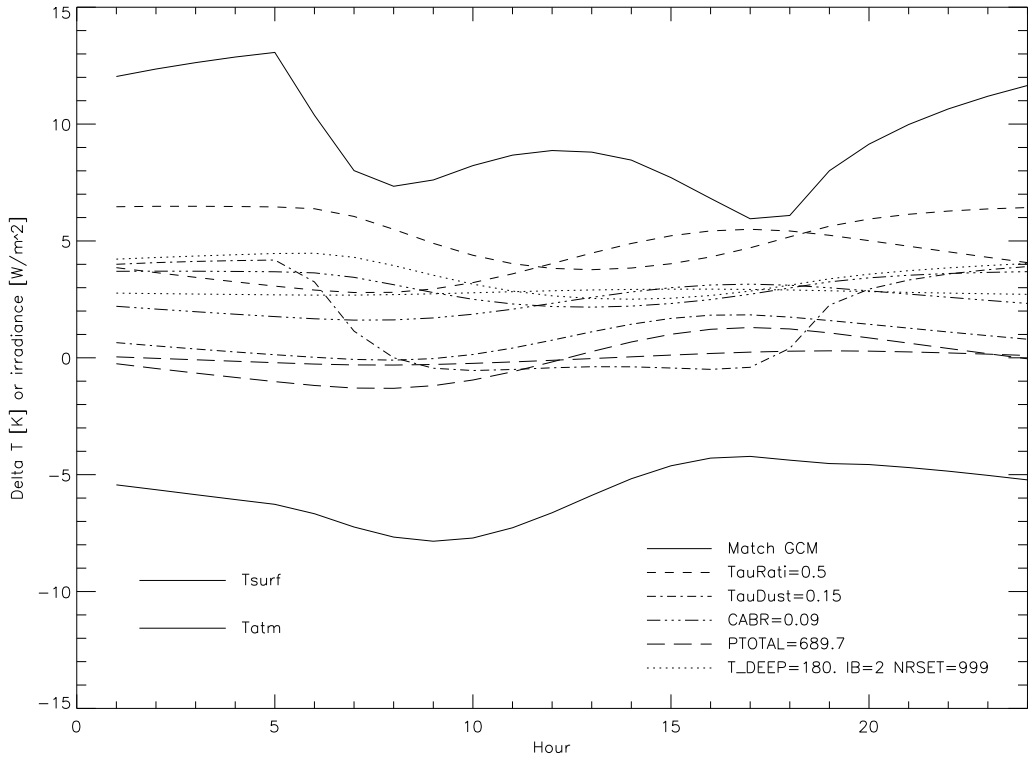

Figure 2: Difference of KRC base model from the GCM model and effect of modifying KRC atmosphere parameters. The solid lines KRC base - GCM temperatures; thick for surface temperature and thin for atmosphere temperature.

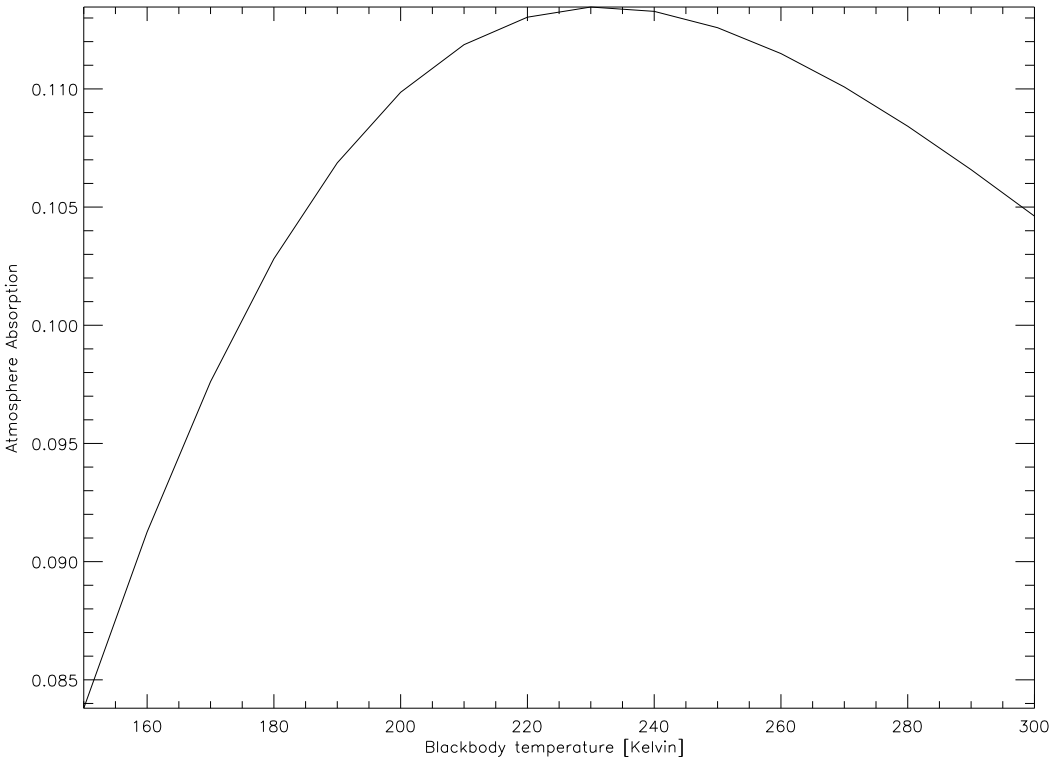

Figure 3: Blocking of thermal radiation by a dust-free Mars atmosphere. Ordinate is the fraction of blackbody radiation absorbed by a nominal atmosphere of 7000[?] Pa $CO_2$with a nominal amount of water vapor. Abscissa is the blackbody temperature.

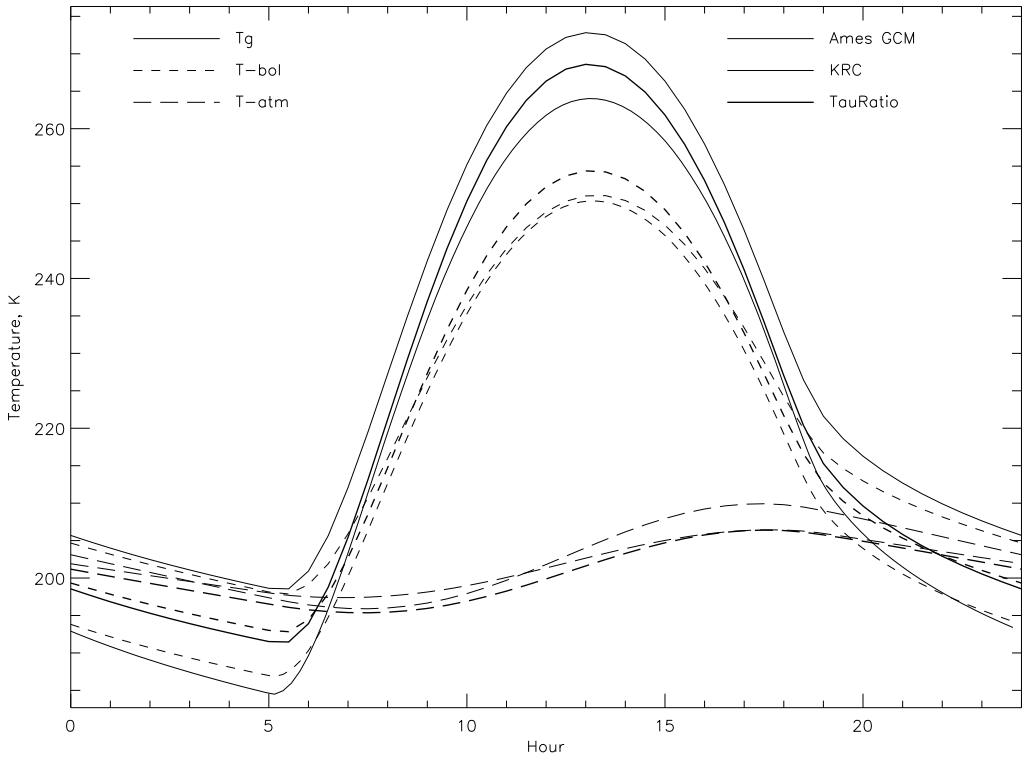

Figure 4: Surface kinetic, mass-weighted atmosphere and planetary model temperatures for the Viking 1 landing site at $L_s = 100°$. Light lines are data from the AMES GCM; heavy lines from KRC. Thermal inertia of 270, surface albedo 0.25.

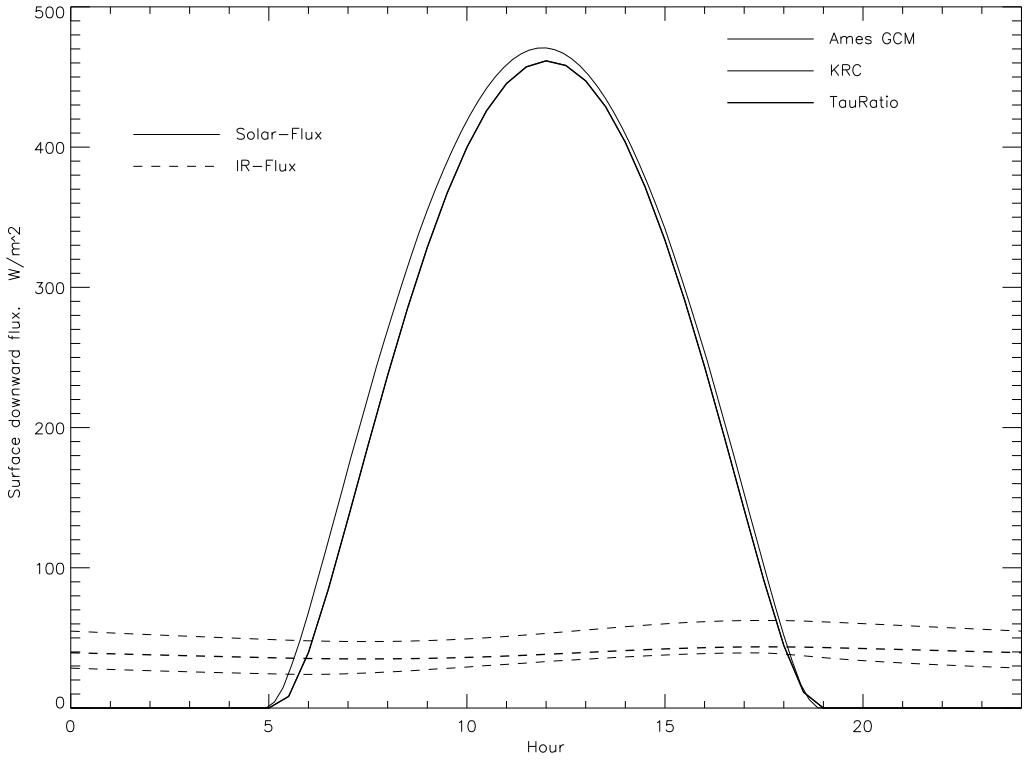

Figure 5: Downward solar and infrared radiation fluxes at the surface for the AMES GCM and KRC (heavy lines) models.

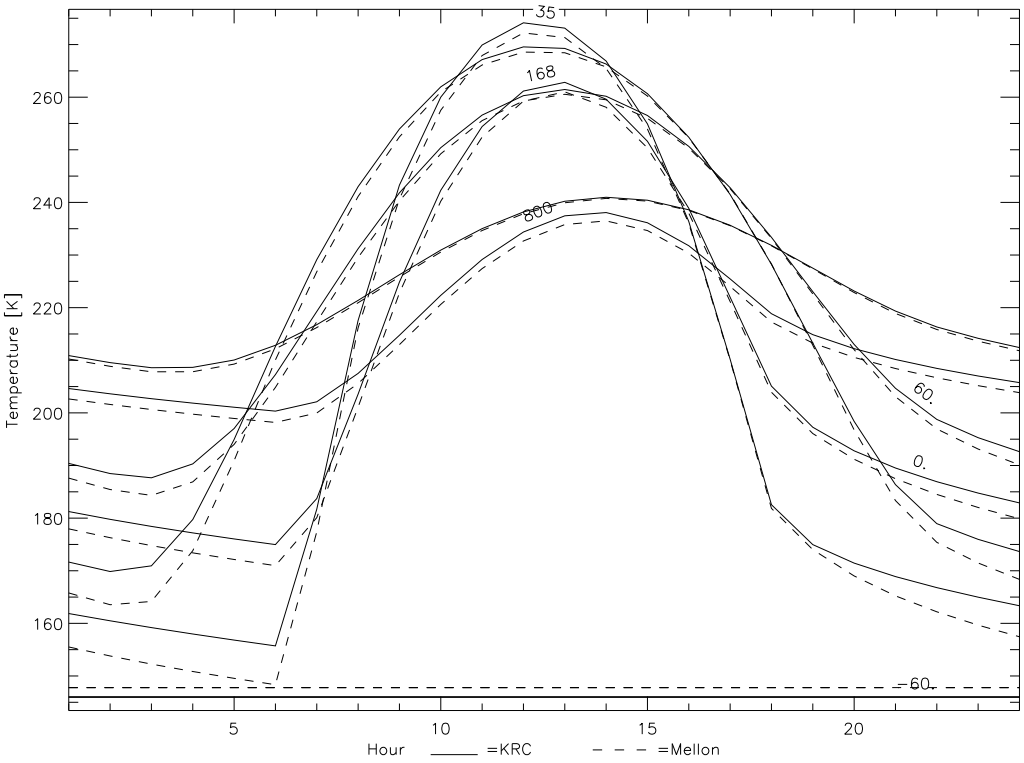

Figure 6: Comparison of KRC with the Mellon models used for TES standard production. Diurnal curves for TI of 35,168 and 800 (labeled for latitude 0) for latitudes 60S, 0 and 60N (labeled for inertia 168), all at $L_s = 100°$. Both models had seasonal frost all day long at 60S. KRC models are a few degrees warmer, the greatest at night and for low thermal inertia.

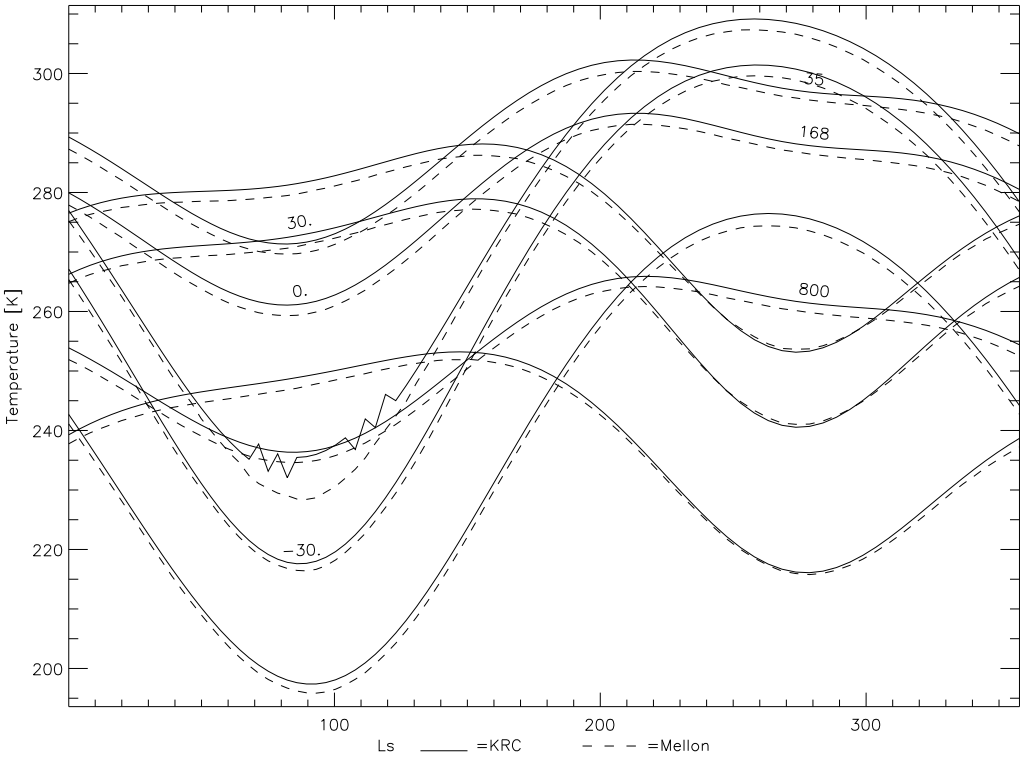

Figure 7: Comparison of KRC with the Mellon models used for TES standard production. Seasonal curves for TI of 35,168 and 800 for latitudes 30S, 0 and 30N, all at 13H. The models track each other closely except for the lowest inertia at 30S near $L_s = 90°$, when CO_2frost forms at night.

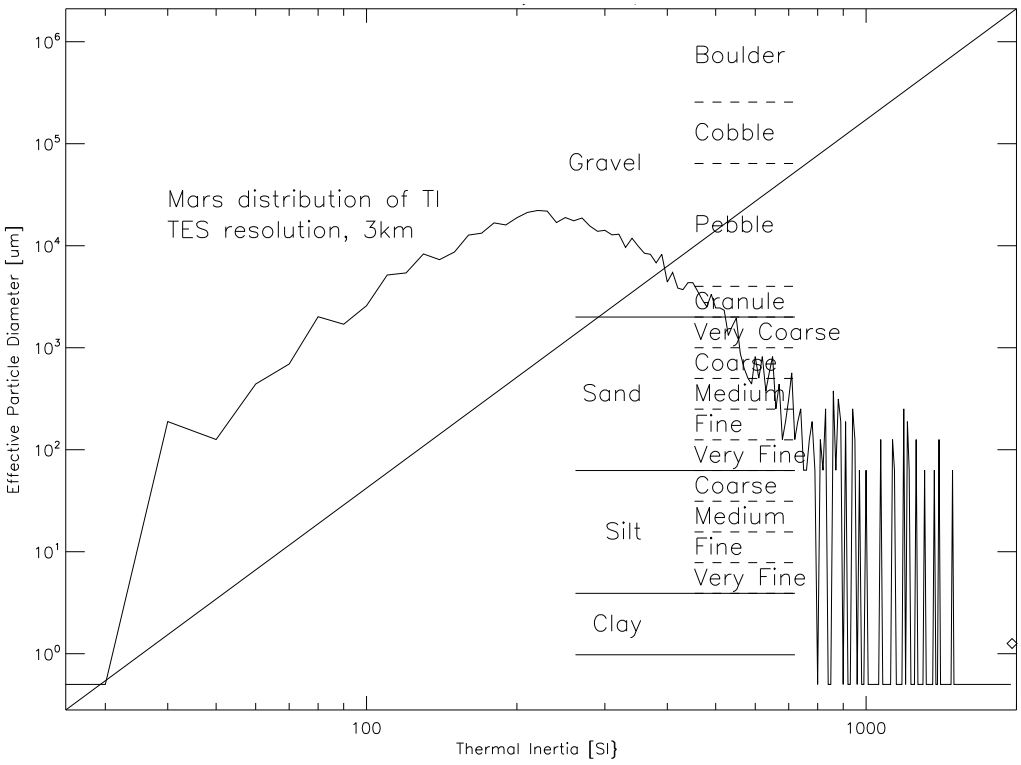

Figure 8: Nominal relation between thermal inertia and effective particle size, shown as the nearly straight line; specific conditions are P=600 Pascal, density=1600 kg/m3 and specific heat=625. The size designations are standard Wentworth scale. The areal distribution of thermal inertia on Mars, between latitudes 80S and 75N is shown as the jagged line, derived from mapping using TES data, [51] Note the log scales; most areas are in TI range of 100:500; values above the peak are increasingly affected by a rock population or real bedrock. The small diamond at high TI indicates the sum of all values above the plotted range.

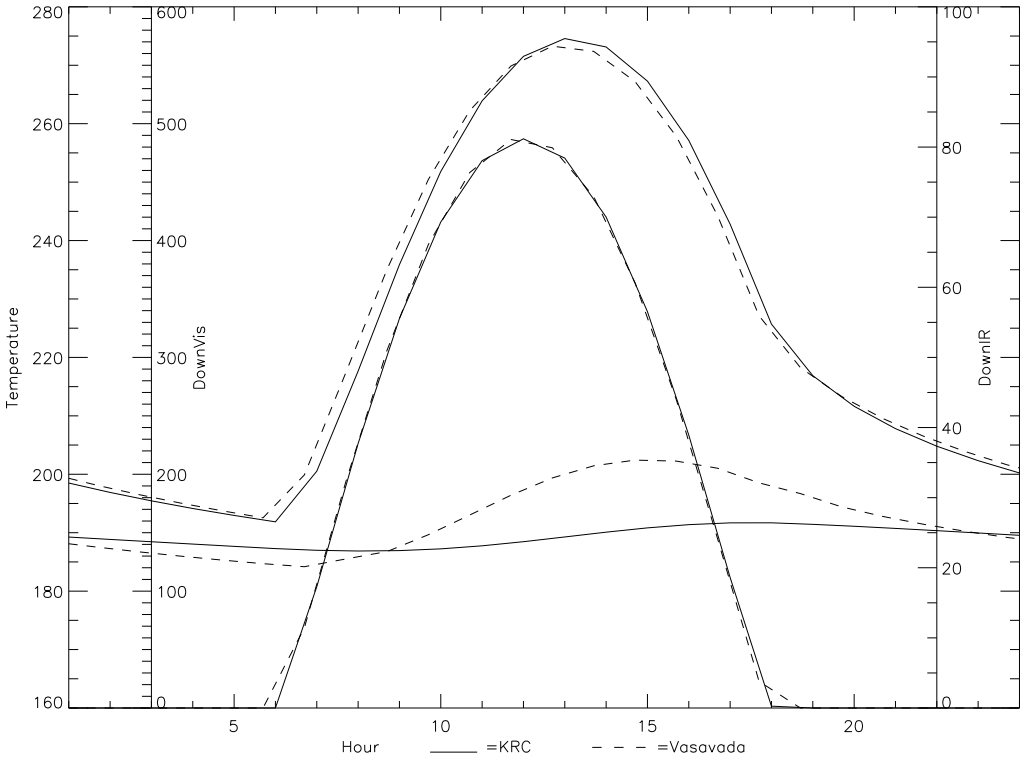

Figure 9: Comparison of KRC (solid lines) with thermal model computed by Ashwin Vasavada (dashed lines). Upper curves are the surface temperature, curves hitting bottom are down-going total insolation at the surface (left auxilliary axis), central curves are down-going infrared radiation at the surface (right auxilliary axis)